CHAPTER 8

PARAGENESIS, FORMATION CONDITIONS, AND FLUID INCLUSION GEOTHERMOMETRY OF ORES

8.1 INTRODUCTION

Following mineral identification and textural characterization, two major objectives in ore microscopy are the determination of the order of formation of associated minerals in time succession, or *paragenesis*, and the estimation of the conditions under which the minerals have formed or have re-equilibrated.[1] Such determinations, although not vital to the extraction or exploitation of the ore, are important in deciphering the geological history of the ore and may be of value in exploration, in correlating various parts of ore bodies, and in the correlation of specific trace metals (e.g., gold) with certain episodes or types of mineralization. Paragenetic determination requires the detailed examination of polished sections to identify phases, recognize diagnostic textures (as described in Chapter 7), and decipher "time diagnostic" features. Doubly polished thin sections can be invaluable in the investigation and interpretation of transparent phases such as sphalerite, and fluid inclusions can yield critical data relating to different stages or changing conditions of ore formation. The application of fluid inclusions is discussed in the latter part of this chapter. Paragenetic interpretation requires well-prepared, representative ore samples, the application of relevant phase equilibria data, and the integration of all geological and mineralogical data available for the deposit.

The sampling and sample examination procedures useful in deciphering paragenesis are also discussed, although not all of the points considered are

[1] "Paragenesis" has also been used, particularly in the European literature, to refer to characteristic ore mineral assemblages but is used in this text only in reference to the sequential formation of minerals.

equally applicable to all ores; indeed, some ores, especially those that have been intensely metamorphosed, are not so amenable to paragenetic studies, either because the original record is insufficiently distinctive or because it has been subsequently altered beyond recognition.

8.2 PARAGENETIC STUDIES

There is no "standard method" for carrying out paragenetic studies, because each ore deposit is unique. However, as the goal of all such studies is to decipher the sequence of mineral formation, certain general principles outlined in the following subsections can be applied to most examples.

8.2.1 Sample Selection and Preparation

The samples available for study rarely comprise more than an infinitesimally small fraction of the total of the deposit; hence, samples must be representative of the whole deposit if they are to be useful in paragenetic studies. Of course, the larger and more complex an ore body is, the greater is the number of samples needed to study it adequately. However, more important than the number of samples is their quality and, in many cases, their orientation—a factor that is especially critical in ores that possess planar or linear features (graded bedding, mineral bands parallel to vein walls, crosscutting mineralized veins, etc.). (See also Chapter 3.) It should be noted that samples of the unmineralized or only slightly mineralized host rocks of a deposit are often as useful as samples of massive ore in deciphering the paragenesis. Such samples can reveal the opaque minerals present before mineralization or those introduced early in the paragenesis. Conventional polished sections may be too small to display textural and paragenetic relationships in very coarse-grained ores, complex veins, or bedded ores; this problem can be overcome by combining hand samples or oriented slabs of ore with polished and thin sections, and by the use of both high- and low-power objectives in microscopy. In some ores, the doubly polished thin section provides information superior to that provided by the conventional polished section for paragenetic studies. It allows observation of gangue and ore minerals in the same sample and of internal structure in some ore minerals (e.g., sphalerite, tetrahedrite, pyrargyrite), which is visible neither in the standard thin section nor the polished section.

It is also necessary to re-emphasize the importance of using well-polished sections. Many subtle features are missed if sections that are poorly polished or that show too much relief are used.

8.2.2 Crystal Morphology and Mutual Grain Boundary Relationships

The shapes of individual crystals and the nature of the contacts between adjacent grains have often been used as criteria for determining paragenesis. In

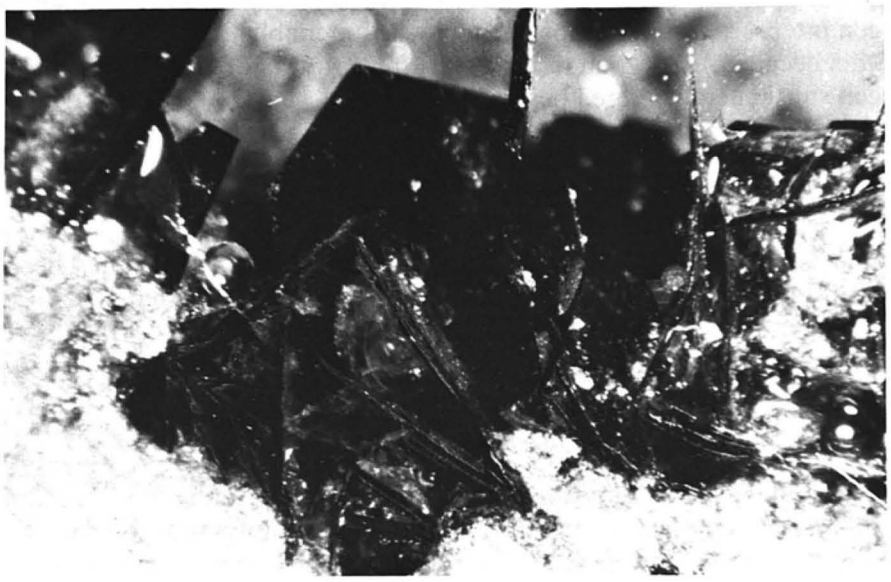

FIGURE 8.1 Euhedral crystals of covellite formed through unobstructed growth into open space. These crystals are embedded in clear epoxy, with the edges of some exposed at the surface of the polished section, Creede, Colorado (width of field = 1 cm).

general, euhedral crystals have been interpreted as forming early and growing unobstructed; grains with convex faces have been interpreted as forming earlier than those with concave faces. Such simplistic interpretations are often correct but must be used with caution. Indeed, for many minerals, euhedral crystal morphology is an indication of growth into open space, especially in vein deposits. For example, calcite, quartz, fluorite, sphalerite, cassiterite, galena, covellite, and sulfosalts usually form well-developed euhedral crystals only in directions in which growth is unobstructed (Figure 8.1). The existence of such crystals, mixed with, or overgrown by, other minerals, indicates that the euhedra were the first formed; furthermore, it usually indicates the direction of general growth (i.e., in the direction of the euhedral crystal faces). However, certain minerals (e.g., pyrite, arsenopyrite) tend, through their force of crystallization, to form well-developed crystals regardless of their position in the paragenetic sequence. For example, early pyrite in Cu-Pb-Zn veins occurs as isolated euhedra or intergrown subhedra with many well-developed faces; secondary pyrite formed as a result of exsolution from primary pyrrhotite in Fe-Cu-Ni ores often occurs as well-formed cubes; pyrite that forms as a result of metamorphic recrystallization commonly occurs as perfectly developed cubic or pyritohedral porphyroblasts up to several centimeters in diameter (Figure 8.2). Furthermore, as discussed in Section 7.7, retrograde metamorphic re-equilibration can result in the release of sulfur by pyrrhotite

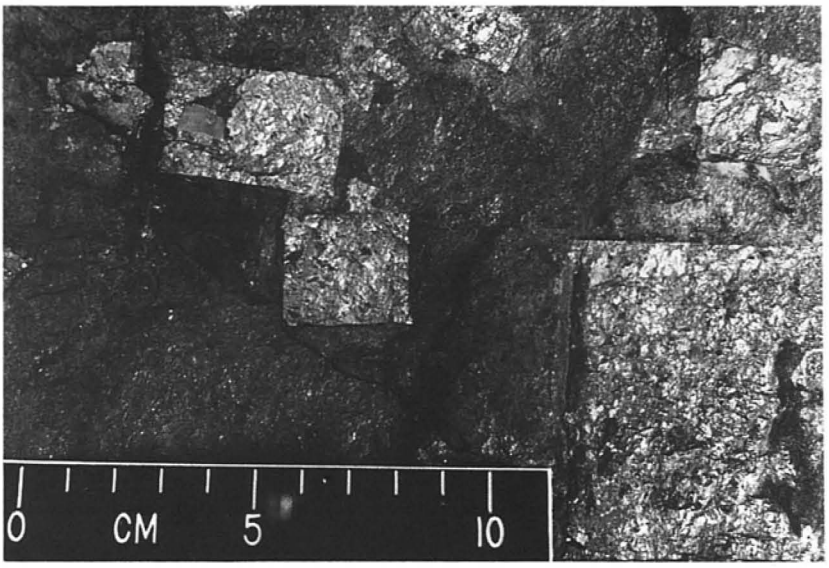

FIGURE 8.2 Porphyroblasts of pyrite grown in a matrix of pyrrhotite during regional metamorphism, Cherokee Mine, Ducktown, Tennessee (centimeter scale).

to form euhedral pyrite crystals. In such a case, the most euhedral crystals were the last, not the first, to form.

Sometimes the evidence of crystal morphology rather than the crystal itself aids in paragenetic interpretation. Thus, in some Pb-Zn ores of the Mississippi Valley, dissolution has removed euhedral 1 cm galena crystals that had grown on the surfaces of open fractures. The evidence of the galena is preserved because, prior to its dissolution, fine-grained pyrite and marcasite were precipitated on top of it in a 2–3 mm thick band. Now the ore specimens reveal the following sequence of events: (1) fracturing of wall rock, (2) formation of sphalerite and euhedral galena, (3) formation of colloform overgrowths of pyrite and marcasite that faithfully record the galena morphology on their undersurface, and (4) leaching, leaving euhedral voids once occupied by the galena.

Mutual grain boundaries (equal degrees of penetration) (Figure 8.3) must be interpreted with care and with the recognition that the ore microscopist has only a two-dimensional view of a three-dimensional material. The equal interpenetration of minerals, the absence of characteristic first-formed crystals, and the absence of replacement features usually prevent determination of any paragenetic sequence and may indicate simultaneous crystallization of the minerals.

8.2.3 Colloform Banding and Growth Zoning

Colloform banding, a concentric botryoidal overgrowth of fine radiating crystal (Figure 8.4a), is a texture that is commonly encountered in open-space fill-

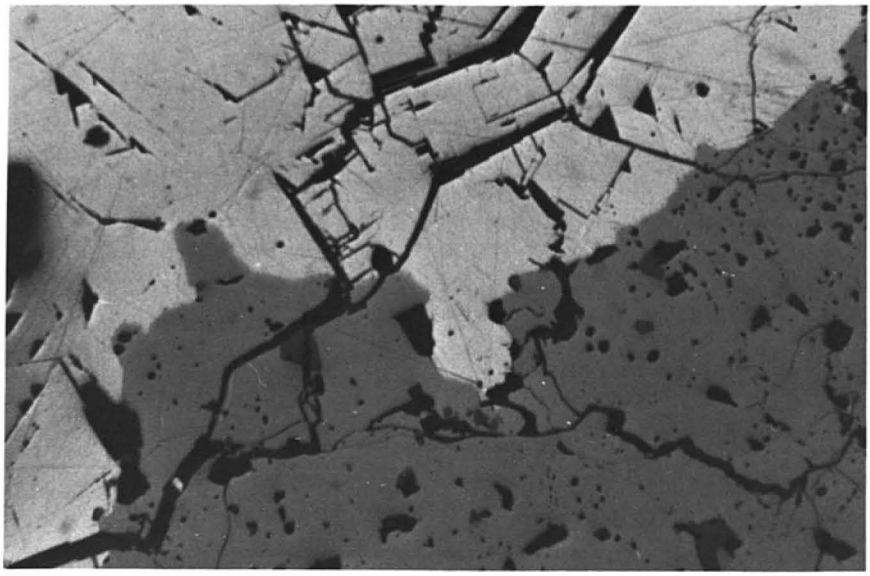

FIGURE 8.3 Mutually interpenetrating grains of sphalerite (medium gray) and galena (white), Montezuma, Colorado (width of field = 520 μm).

ing ores. It is especially common in iron and manganese oxides (Figure 8.4b), including manganese nodules, uranium minerals, arsenides, and in pyrite and sphalerite. Although colloform banding has often been attributed to formation from a gel, Roedder (1968) has shown that typical colloform sphalerites owe their origin to direct crystallization of fine fibrous crystals from a fluid. The colloform bands are actually composed of radiating masses of crystals growing from many adjacent sites along a vein wall, the surface of a wall-rock fragment, or previously formed ore minerals. Although generally forming a smooth or undulating surface, colloform growth may occur locally as stalactites. Several Mississippi Valley and vein-type Zn-Pb deposits have also yielded well-developed sphalerite stalactites, complete with the hollow central tube. The colloform structures grow from some substrate outward, with sequential growth periods evidenced by overlying bands. Individual bands are often distinguished by interlayering with other minerals (or even organic inclusions), by change in the size, shape, or orientation of crystals, or by color zoning, each of which represents some change in the ore fluid or the conditions of precipitation. Minor chemical changes, as evidenced by micron-scale color banding in colloform sphalerites (only seen in doubly polished thin sections in transmitted light), do not disturb crystal growth, since individual crystals exhibit continuity for 1–2 cm and may contain hundreds of bands growing across them.

Growth zoning in individual crystals is a common feature in many types of ore minerals and in a wide variety of deposits. Magmatic precipitates, such as

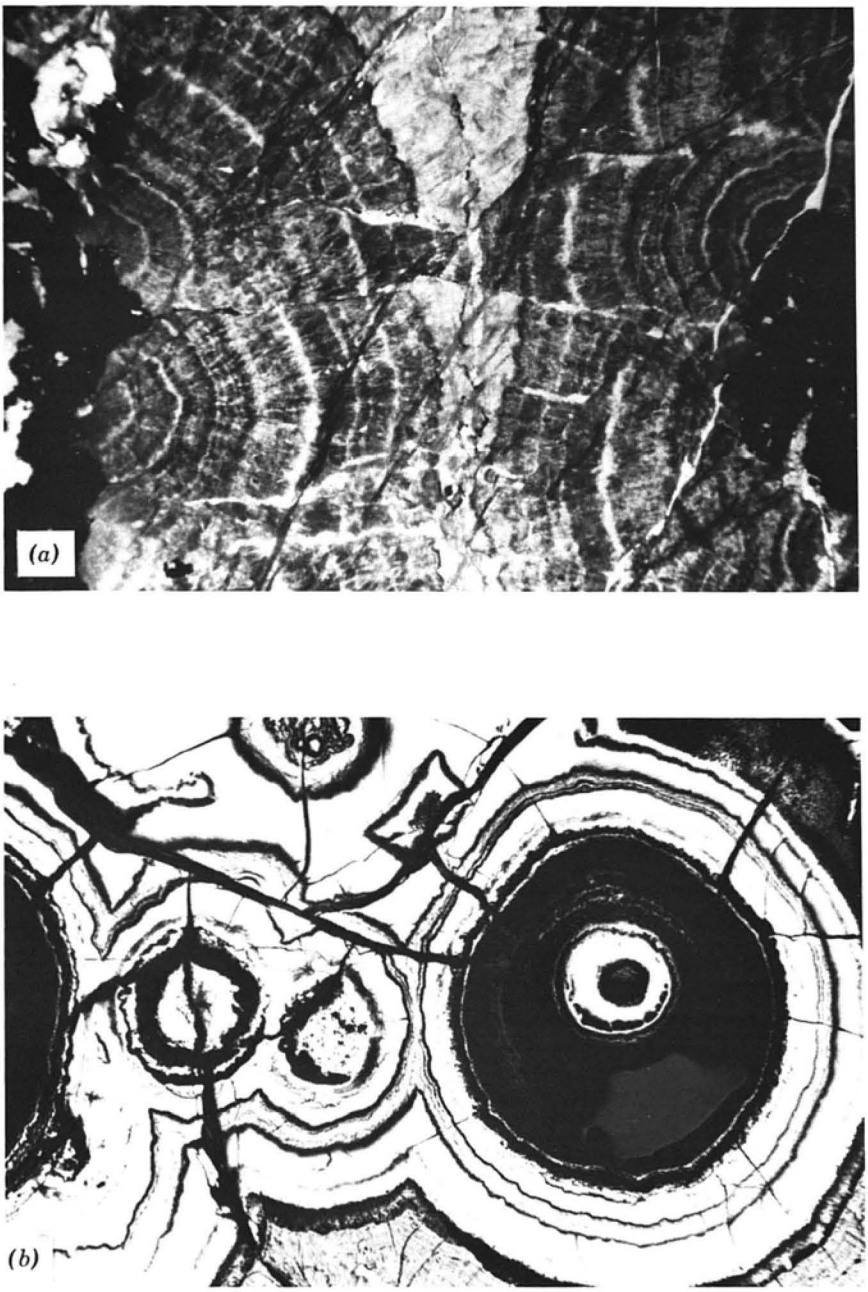

FIGURE 8.4 (*a*) Colloform banding illustrating sequential growth of sphalerite inward from the walls of a fracture; transmitted light photomicrograph of doubly polished thin section. Early pyrite (black) has been successively overgrown by banded sphalerite and dolomite (white), Austinville, Virginia (width of field = 2,000 μm). (*b*) Concentric growth banding, showing sequential development of hematite and goethite in pisolitic iron ore, Schefferville, Quebec (width of field = 2,000 μm).

chromites and magnetites, may display zonal compositional and color variations, reflecting changes in the magma from which they precipitated. Several hydrothermally deposited vein minerals may contain distinct color bands (Figure 7.4), which also record a changing environment of formation. Such bands often contain fluid or solid inclusions trapped at the time of precipitation and thus can yield considerable paragenetic information.

The existence of the same, or at least portions of the same, color or compositional zonal sequence in adjacent sphalerite crystals or in crystals growing simultaneously along a fracture provides the basis for *sphalerite stratigraphy* (a term coined by Barton et al., 1977). McLimans, Barnes, and Ohmoto (1980), have applied sphalerite stratigraphy in the Upper Mississippi Valley District by correlating individual color bands in colloform sphalerite over a few hundred meters and certain bands over several kilometers (Figure 8.5). Sphalerite stratigraphy is a powerful technique in paragenetic studies but requires carefully collected, preferably oriented specimens, and their examination in doubly polished thin sections.

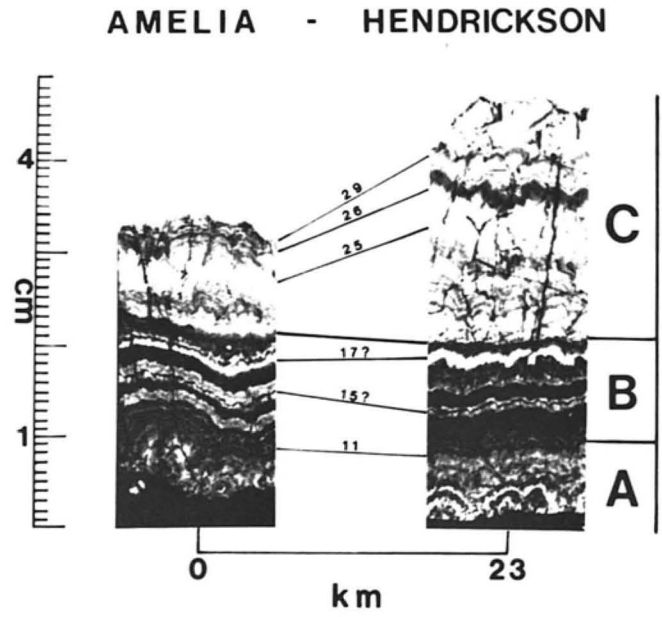

FIGURE 8.5 Polished thin sections of sphalerite showing stratigraphic zones A (early), B (middle), and C (late), and correlation of stratigraphy over 23 km northeast from the Amelia orebody, Illinois (left), to the Hendrickson orebody, Wisconsin (right). (Reproduced from R. K. McLimans et al., *Econ. Geol.* **75**, 354, 1980, with permission of the authors and the publisher.)

8.2.4 Cathodoluminescence and Fluorescence

In recent years, cathodoluminescence microscopy has become a useful ancillary technique in paragenetic studies of certain minerals. In this technique, a 1 cm diameter beam of electrons accelerated at a potential of 10–15 kv strikes a sample (thin section or polished section) contained in an evacuated viewing chamber on a microscope stage. The sample may be viewed in transmitted or reflected light, or only by the luminescence excited by the electron beam. Although most ore minerals exhibit no visible response to the electron beam, some ore minerals such as cassiterite, sphalerite, scheelite, powellite, and willemite, and some common gangue minerals such as fluorite, calcite, dolomite, feldspar, and quartz (Marshall, 1988; Barker and Kopp, 1991)), emit visible light luminescence. The luminescence of these minerals depends on the presence of trace to minor amounts of an activator element (e.g., Mn, Dy, Cr) incorporated at the time of initial crystallization.

Because the fluids depositing both ore and gangue minerals commonly change as a function of time, sequentially deposited ore and gangue minerals sometimes possess luminescent growth zones that are not visible either using transmitted- or reflected-light microscopy (Figure 8.6). These growth zones may be useful in sample-to-sample correlation and in the interpretation of paragenesis. The technique has been extensively used in the study of sedimentary cements (Meyers, 1978; Nickel, 1978) and has proved to be effective in the correlation of carbonate gangue associated with sphalerite ores in the East Tennessee zinc district (Ebers and Kopp, 1979).

Fluorescence, the emission of visible light in response to exposure to ultraviolet (UV) light, is very similar to cathodoluminescence and thus provides another means by which paragenetic information may be derived from polished or thin sections. UV light sources, usually mercury arc lamps ("black lamps"), are generally divided into long-wave (300–400 nm) and short-wave (<300 nm) varieties and are available as inexpensive handheld and more elaborate microscope-mounted models. Most common ore and gangue minerals exhibit no visible response to UV light, but many of the same minerals noted above as being cathodoluminescent also fluoresce visibly, especially under short-wave UV light. The name, in fact, is derived from the fluorescence of fluorite. As with cathodoluminescence, fluorescence depends upon the presence of certain activator elements and varies widely in intensity and color.

Routine examination of samples with a UV lamp is very simple and often leads to the immediate recognition of some minerals (e.g., powellite, cassiterite, scheelite) that do not have other unique distinguishing characteristics. Furthermore, characteristic broad growth or alteration zones (e.g., fluorescent bands in calcite, fluorite, dolomite) and sometimes delicate growth zoning, invisible under normal lighting conditions, may become visible. Such zoning may, of course, be very useful in the correlation of one sample with another. The simplicity of use and the widespread availability of UV lamps, combined

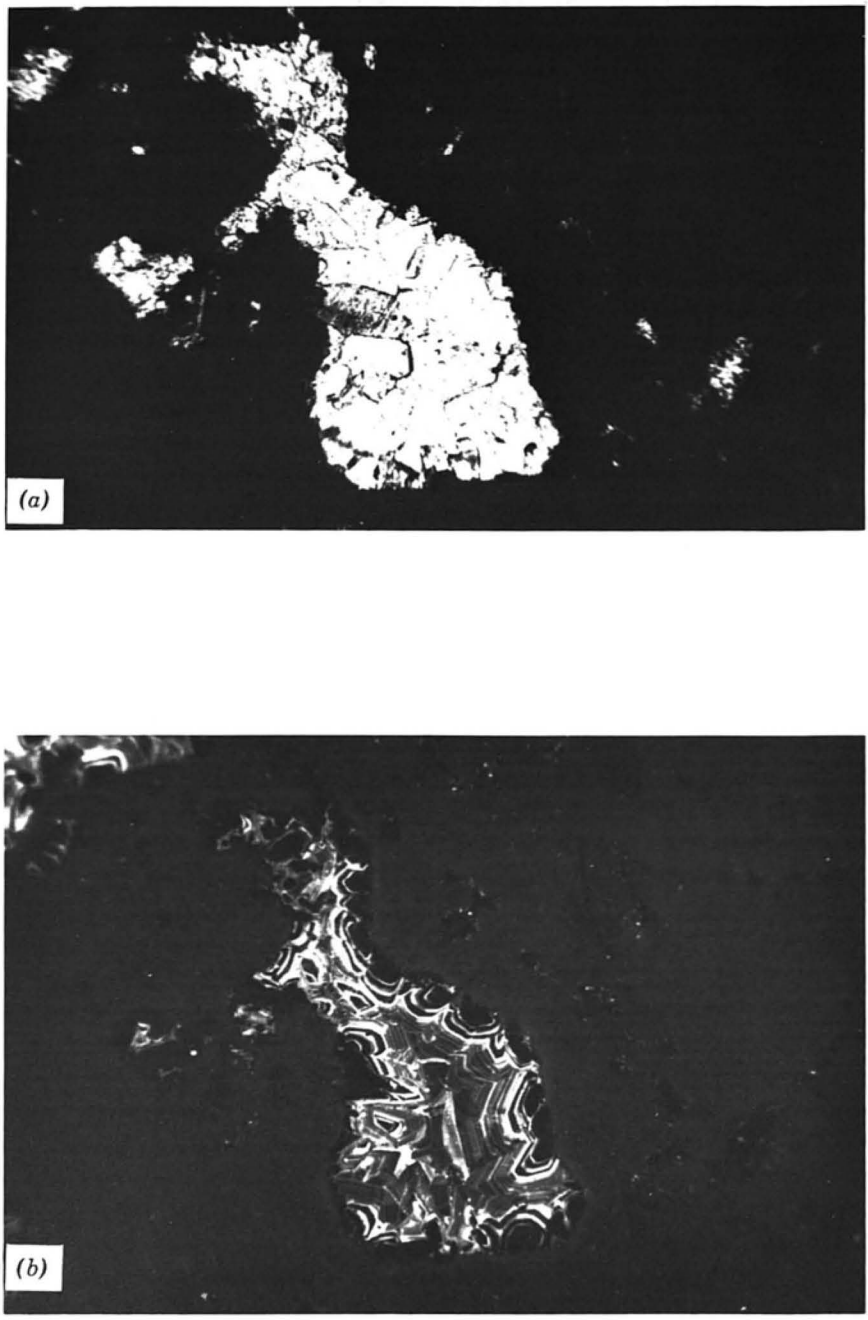

FIGURE 8.6 The use of cathodoluminescence in defining growth banding in calcite: (*a*) a thin section with a calcite-filled vug as viewed in transmitted plane polarized light; (*b*) the same area under cathodoluminescence reveals the delicate growth zoning as defined by differing brightness of the bands (width of field = 4,400 μm).

with the ease of obtaining valuable information, has made this technique a routine tool in many laboratories.

8.2.5 Crosscutting Relationships

In mineralogical examination, just as in geological field studies, crosscutting relationships are a key to paragenetic interpretation. The *veinlet or other feature that crosscuts another is younger than that which it cuts across*, except when the older phase has been replaced, or when both features result from metamorphic remobilization. Therefore, the veinlet that cuts across another veinlet (Figure 8.7), or crystal, is later in the paragenetic sequence, whether it represents simple open-space filling or replacement. Deformational episodes are often indicated by the presence of microfaults (Figure 8.4a), which offset bands or veins of earlier-formed minerals, or by the crushing of earlier grains that may have been subsequently infilled by later minerals. Detailed studies of some syngenetic ores (i.e., those in which ore and host rock minerals are believed to have formed at the same time) have revealed crosscutting relationships in the form of scour marks, channels, soft sediment slumping, and crossbedding, some of which may be observed on the microscale.

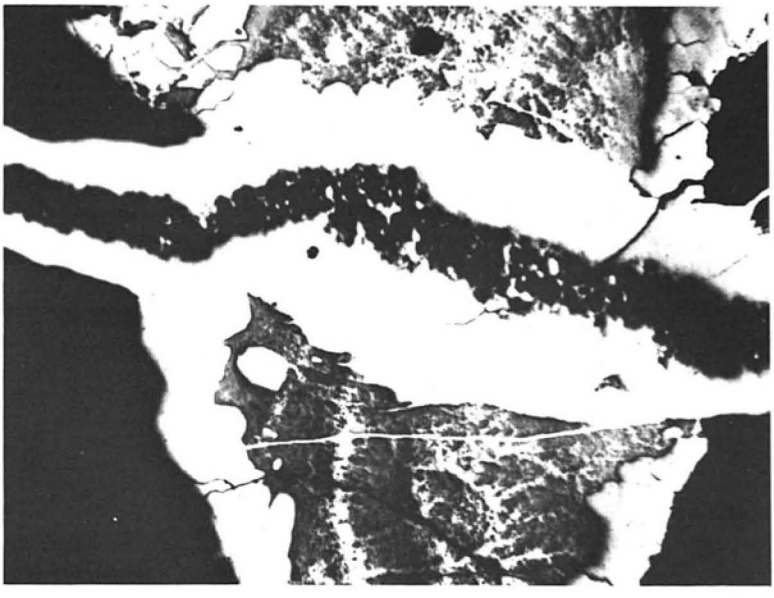

FIGURE 8.7 Crosscutting relationships shown in a manganese oxide ore in which early chalcophanite is cut by a later veinlet of the same mineral, Red Brush Mine, Virginia (width of field = 2,000 μm).

8.2.6 Replacement

Replacement features are very useful in the determination of paragenesis; clearly, the mineral being replaced predates the one replacing it. Since replacement is generally a surface chemical reaction, it usually proceeds inward from crystal boundaries or along fractures. In general, during advanced replacement, the replacing phase possesses convex boundaries, whereas the replaced phase possesses concave boundaries and may remain as residual "islands" within a matrix of the later phase (Figure 7.11c). Replacement and weathering processes often lead to one mineral occupying the site originally occupied by another in the paragenesis; the difficulty often lies in the "identification" of the now absent mineral. Sometimes, replacement has been incomplete and a few fragments of the original phase remain. A good example is illustrated in Figure 9.8, in which some original pentlandite remains within the replacing violarite; most of the pentlandite grains in this ore are completely replaced, but the grain shown reveals the true paragenesis. The cubic morphology of pyrite is probably the most readily recognized of replaced minerals; thus, cubes of chalcopyrite, covellite, or goethite are usually regarded as pseudomorphs after pyrite. Similarly, in Figure 7.10b, characteristic bladed crystals of marcasite have been partly replaced by goethite.

8.2.7 Twinning

Twinning can be useful in the interpretation of both the paragenesis and the deformational history of an ore. Twinning may form during initial growth, through inversion, or as a result of deformation (Figures 7.19, 7.20, and 7.21). Since growth twinning is a function of temperature and degree of ore fluid supersaturation and since kinetics are also influenced by the crystallization, the presence of twinning in only some grains of a specific mineral may be useful in distinguishing different generations of that mineral. Inversion twinning, if unequivocally identified, is indicative of the initial formation of a higher temperature phase and of at least partial re-equilibration on cooling. Deformational twinning can serve as an indicator of deformation during the ore-forming episode (if present only in early formed minerals) or after ore deposition (if present in the ore minerals of all stages).

8.2.8 Exsolution

Exsolution is common in some ore types and may be useful in deciphering certain stages of the paragenesis. In the Fe-Cu-Ni (-Pt) ores associated with ultramafic rocks (Section 9.3), virtually all of the nickel remains incorporated within the $(Fe, Ni)_{1-x}S$ monosulfide solid solution from the time of initial formation at 900–1100°C until the ores cool below 400°C (Figures 9.6 and 9.7). Laboratory phase equilibria studies demonstrate that much of the nickel then exsolves as oriented lamellae of pentlandite. The origin of the earliest exsolved pentlandite is not immediately obvious, because it coalesces to form chain-

like veinlets (Figures 8.8a and 9.5) at the margins of the host pyrrhotite grains; however, the later (and lower temperature) exsolved pentlandite is retained within the pyrrhotite as crystallographically oriented lamellae and "flames" (Figure 8.8b). These characteristic exsolution lamellae indicate that the pentlandite is a secondary phase formed later than the pyrrhotite; although the phase equilibria indicate that this is also true of the granular vein pentlandite, it is not obvious from the texture.

8.3 EXAMPLES OF PARAGENETIC STUDIES

Although it is difficult to generalize, the opaque minerals in many ores can be associated with one of four major divisions:

1. The host rock (or wallrock) materials, which, if igneous, may contain primary oxides or which, if sedimentary, may contain detrital or authigenic opaques (e.g., framboidal pyrite, titanium oxides).
2. The main mineralization episode, which, although often multiphase, is usually one major introduction of fluids, volatiles, or magma that then undergo cooling.
3. A phase of secondary enrichment (in the zone of supergene alteration) resulting in overgrowths and replacement textures.
4. A phase of oxidation and weathering, again resulting in replacement textures and the formation of oxides, hydroxides, sulfates, carbonates, and so on.

Normally the sequence of mineral formation (paragenesis) would follow divisions (1) through (4), although many deposits contain evidence of only divisions (1) and (2). It is also important to note that many minerals may have more than one paragenetic position, although different generations may have different habits (e.g., very early pyrite framboids →pyrite cubes → late colloform pyrite) or chemical compositions.

The mineralogical literature contains many paragenetic studies undertaken in varying amounts of detail. Here, four different types of ores are used as examples of what can be achieved through careful observations and application of available data.

8.3.1 The Nickel-Copper Ores of the Sudbury District, Ontario

The paragenetic sequence of the minerals in the massive nickel-copper ores of the Sudbury basin has become apparent through the combination of field, microscopic, and phase equilibrium studies. The setting of these ores, at the base of a mafic intrusive body, led to the view that they are a product of the intrusive episode. The common trend of massive ore grading upward into disseminated ore, in which isolated "droplets" of sulfide are suspended in a sili-

cate matrix, suggests that the sulfides—pyrrhotite with lesser amounts of pentlandite, chalcopyrite, pyrite, and magnetite—had their origin as immiscible sulfide melts, which, after separation from the parent silicate magma, coalesced at the base of the intrusion through gravitational setting. Subsequent discovery of similar sulfide droplets (Figure 7.2b) in crusts on basaltic lava lakes in Hawaii and in pillow lavas on midocean ridges, and laboratory studies on the solubility of sulfur in ultramafic melts, confirm the possibility of this general mode of origin. Although direct separation and segregation of a sulfide melt is no doubt the means by which many Sudbury-like ores have formed, current theories for the origin of the Sudbury ores involve a more complex history with several phases of injection of sulfide- and silicate-rich magmas that had already undergone some differentiation (Naldrett, 1989).

The first mineral to crystallize from the Sudbury sulfide-oxide melts was magnetite, which formed as isolated skeletal to euhedral or subhedral grains (Figure 8.8a). Subsequent to the onset of magnetite crystallization, all or most of the sulfide mass crystallized as a nickel- and copper-bearing, high-temperature, "pyrrhotite-like" phase (the *mss*, monosulfide solid solution, as shown in Figures 9.6 and 9.7). The phase equilibrium studies of Yund and Kullerud (1966) and Naldrett, Craig, and Kullerud (1967) have demonstrated that, during subsequent cooling, the mss could not have continued to accommodate the copper and nickel in solid solution. Expulsion of the copper as a high-temperature chalcopyrite-like phase (the *iss*, intermediate solid solution) probably would have begun when temperatures cooled to 400–500°C; most of the copper would have been expelled before cooling reached 300°C, but small amounts would have continued forming from the mss as cooling reached 100°C or less. Exsolution of nickel, in the form of pentlandite, would have begun as soon as the sulfur-poor boundary of the shrinking mss (Figure 9.7) reached the bulk composition of the ore in any local region. Pentlandite is not stable above about 610°C (pentlandite decomposes to mss + heazlewoodite, Ni_3S_2, above this temperature), but a plot of the bulk compositions of most nickel-copper ores, including those at Sudbury, indicates that pentlandite formation would not have occurred above about 400°C. In laboratory studies (Francis et al., 1976; Kelly and Vaughan, 1983), the expulsion of nickel as pentlandite occurs as crystallographically oriented lamellae in the mss. However, during the slow cooling from 400° down to ~100°C, the previously expelled chalcopyrite-like phase would have tended to coalesce into anhedral masses (Figure 8.8a) and the pentlandite would have tended to diffuse and recrystallize into chain-like veinlets interstitial to mss grains. During continued cooling at temperatures below 100–200°C, the diffusion rates of nickel would be much reduced and the last pentlandite exsolved would be trapped as fine-oriented "flames" (Figure 8.8b). Locally, the cooling iss phase would exsolve cubanite (Figure 8.8c) and would recrystallize as chalcopyrite.

The paragenetic position of pyrite, which is irregularly distributed in the Sudbury ores, would have depended on the local bulk sulfur content of the sulfide mass (see Figures 9.6 and 9.7); however, its tendency to form euhedral

crystals now masks its position in the sequence. If the local sulfur content were less than about 38 wt %, pyrite would not have formed from the mss until the ores cooled below 215°C and much pentlandite had been exsolved. However, if the local sulfur content were more than about 39 wt %, pyrite would have begun forming when the sulfur-rich boundary of the mss retreated to the local bulk composition. In either situation, the pyrite and pentlandite would not have coexisted until the temperature had cooled below about 215°C (Craig, 1973).

The pyrrhotite of the Sudbury ores consists of a mixture of hexagonal and monoclinic forms and represents the low-temperature remnant of the mss after the copper and nickel have been exsolved as iss (or chalcopyrite) and pentlandite. As is evident in Figure 8.9, these two forms of pyrrhotite formed only after cooling of the ores was nearly complete.

The last stage in the paragenesis of the Sudbury nickel-copper ores was the local development of violarite as an alteration product of pentlandite (and sometimes pyrrhotite) (Figure 8. 8d). The formation of violarite from pentlandite probably does not reflect an equilibrium state but a situation in which the pentlandite structure is converted to the violarite structure as iron and nickel are removed during weathering.

The paragenesis of the Sudbury ores is summarized in Figure 8.9; the mss and iss are noted in parentheses, because their role is reconstructed from studies of phase equilibria.

8.3.2 Tin-Tungsten Ores in Bolivia

In a detailed study of the mineralogy, paragenesis, and geothermometry of Bolivian tin-tungsten vein ores, Kelly and Turneaure (1970) have unraveled a complex history of ore formation. These ores are interpreted as subvolcanic vein deposits formed at depths of 350–2,000 m and in a temperature range of 530–70°C. The ore solutions, as evidenced by fluid inclusions, were NaCl-rich brines of low CO_2 content that were boiling during at least part of the ore-forming period. The paragenetic sequence is summarized in Figure 8.10.

In the earliest vein stage, quartz with apatite intergrown as a coarse band along the vein walls is observed, quartz being overgrown by cassiterite, which makes up the central part of the vein and which lines cavities with well-developed crystals (Figure 8.11a). Local bismuthinite is interpreted as having crystallized before cassiterite because it is both surrounded and replaced by the cassiterite. In the base metal sulfide stage, pyrrhotite stannite and sphalerite fill space between and partly replace quartz and cassiterite (Figure 8.11b). The sphalerite contains exsolved stannite as well as "chalcopyrite disease," indicating modification by later copper- and iron-bearing solutions. Early fluorite is mutually intergrown with sphalerite and pyrrhotite (Figure 8.11c). The pyrite-marcasite-siderite stage is evidenced by pyrrhotite alteration (Figure 8.11d); the hypogene nature of the alteration is demonstrated by high-filling temperatures of fluid inclusions in siderite. Pyrrhotite alteration begins

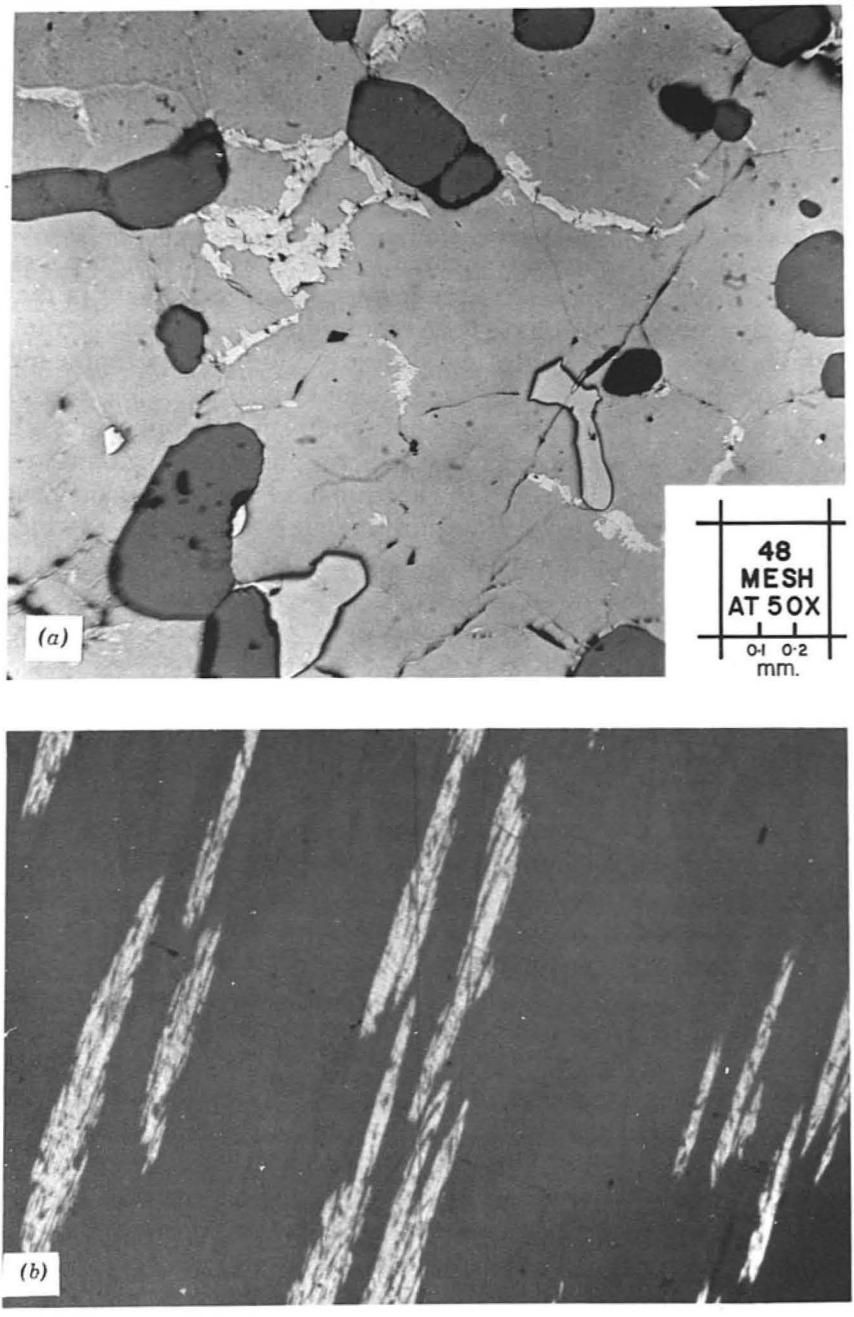

FIGURE 8.8 Nickel-copper ore from Sudbury, Ontario, Canada, illustrating the paragenesis of the ore. (*a*) Early-formed subhedral grains of magnetite (dark gray) within coarse granular pyrrhotite (medium gray), rimmed by granular pentlandite that has coalesced after exsolution. Also present are two anhedral grains of chalcopyrite (width of field = 1,700 μm). (*b*) Exsolutlon "flames" of pentlandite (light gray) in a

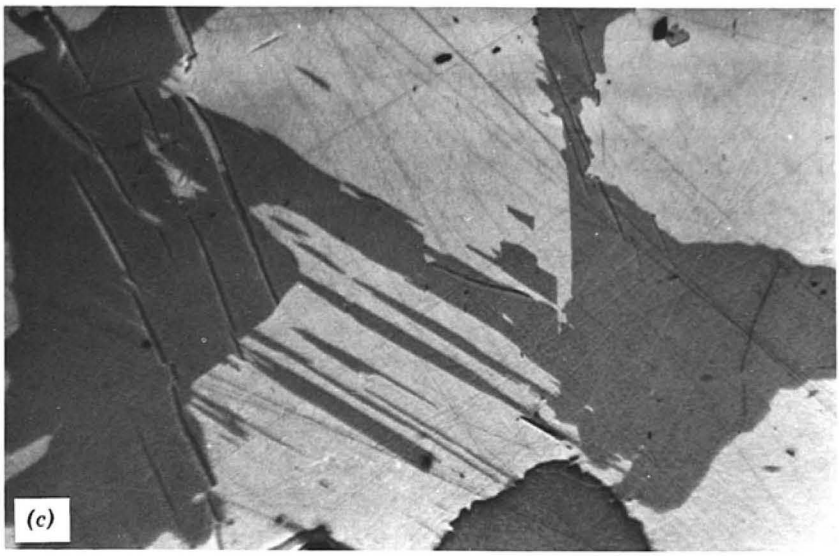

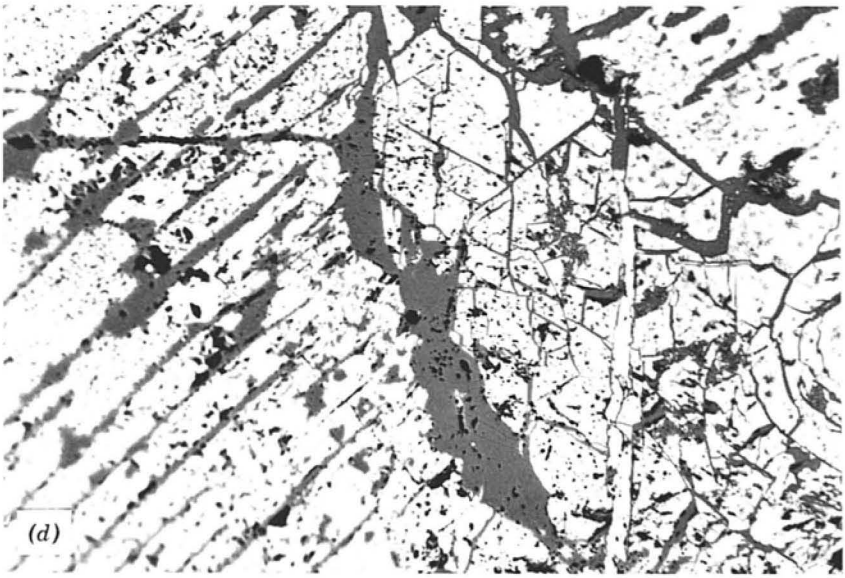

pyrrhotite matrix (width of field = 330 μm). (*c*) Irregular areas and lamellae of cubanite (dark gray) within chalcopyrite produced by exsolution on breakdown of iss (crossed polars) (width of field = 330 μm). (*d*) A veinlet of violarite retaining the blocky fracture pattern of the pentlandite that it has replaced. It is surrounded by altered pyrrhotite that exhibits a single cleavage direction. (width of field = 520 μm).

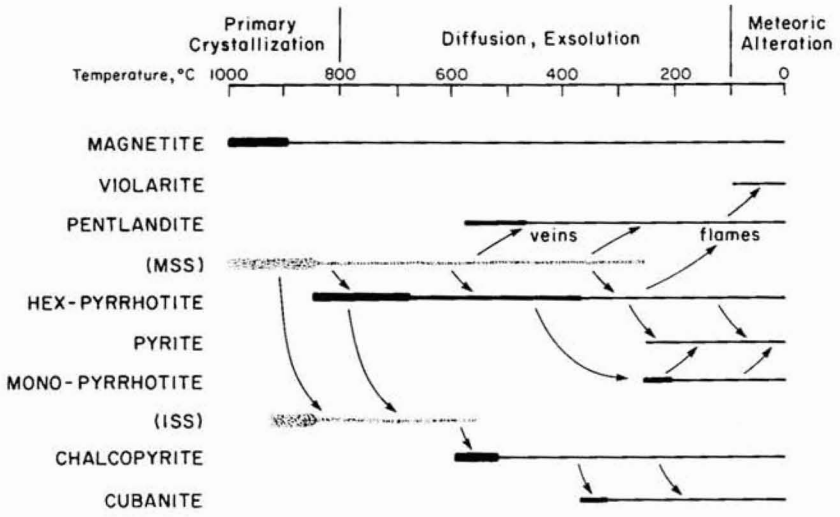

FIGURE 8.9 Paragenetic diagram of the Sudbury, Ontario, Ni-Cu ores. The medium or heavy weight black line indicates the period of formation; the light weight black line indicates persistence; the stippled lines indicate phases that exist only at elevated temperatures.

along veins and fractures but may proceed to perfect pseudomorphs of pyrite-marcasite after pyrrhotite crystals. The final stages evident in the paragenesis are veinlets and crustifications of (1) siderite, sphalerite, and late fluorite; and (2) hydrous phosphates. In Figure 8.10, Kelly and Turneaure (1970) trace the general paragenesis and the thermal history of the ores.

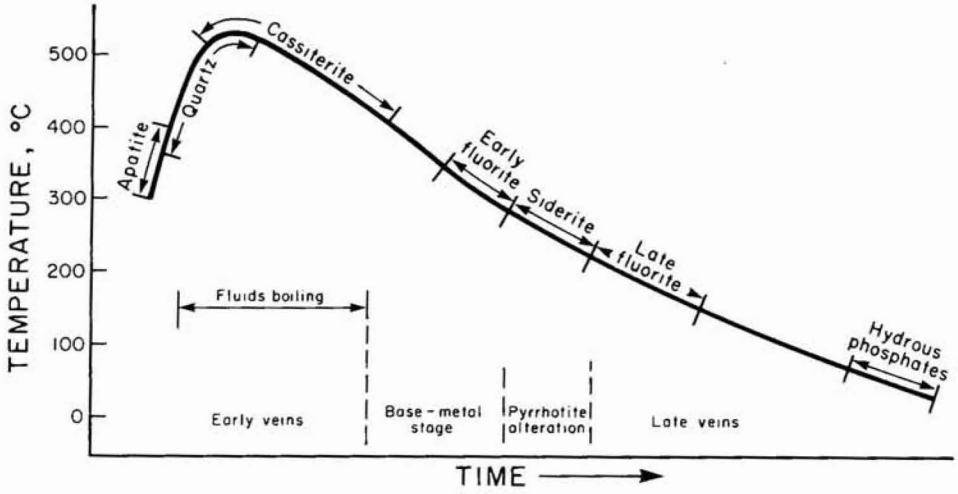

FIGURE 8.10 Summarizes the stages of formation and temperature variation during deposition of the tin-tungsten ores of Bolivia. (After Kelly and Turneaure, *Econ. Geol.* **65**, 673, 1970; used with permission.)

8.3.3 The Lead-Zinc Ores of the North Pennines, England

The North Pennine Orefield contains lead-zinc-barite-fluorite mineralization, chiefly as fissure-infilling veins in mainly lower carboniferous strata. Fluid inclusion studies suggest that the solutions responsible for the precipitation of these minerals were brines and that deposition occurred at temperatures below 250°C.

The sulfide mineral assemblages of the North Pennines were studied by Vaughan and Ixer (1980), who noted distinct differences in the assemblages to the north in the Alston Block area and to the south of the orefield in the Askrigg Block. In the latter area, a consistent generalized paragenesis is observed, as shown in Figure 8.12. An early diagenetic phase of framboidal pyrite is found in the host rock limestone and is intimately associated with small carbonaceous laths. These pyrite framboids may act as nuclei to later pyrite cubes or radiating marcasite crystals (Figure 8.13a). Bravoite, the earliest epigenetic sulfide, may show multiple zoning and occurs as inclusions in fluorite, calcite, or barite (Figure 8.13b). Bravoite is commonly succeeded by nickeliferous pryite and the first of several generations of normal pyrite that is intergrown with marcasite and nickeliferous marcasite (Figure 8.13c). Minor chalcopyrite (showing later supergene alteration to covellite and limonite) is followed by galena, which can enclose all of the earlier sulfides (Figure 8.13d) and commonly alters in weathering to cerussite or anglesite. Sphalerite is the last primary sulfide to form.

This overall paragenesis is very similar to that observed in the South Pennine Orefield, whereas, in the northernmost Alston Block area, much greater diversity was found. The authors discuss the observed paragenesis in terms of the conditions of ore formation, which suggest higher temperatures and more diverse fluid compositions in this northernmost area.

8.3.4 Gold and Base-Metal Ores of the Mashan District, China

The Tongling District of Anhui Province in southeast central China hosts stratiform massive to disseminated base-metal and gold-bearing sulfide deposits that have been mined intermittently since the Ming Dynasty (1348–1644 A.D.). The ores occur as disseminated to massive replacements of limestones, especially at flexure zones, where the dip of the beds changes markedly.

Detailed studies of the ore mineralogy have revealed a complex multistage paragenesis involving iron and base-metal sulfides, tellurides, and gold; this is summarized in Figure 8.14. There are seven distinguishable mineralization stages and a clear phase of brittle deformation; several of these are illustrated in Figures 8.15 and 8.16. Limited fluid inclusion data indicate that ore formation occurred at about 300°C.

The massive sulfide ores consist of dominant pyrite, arsenopyrite, and pyrrhotite, with significant amounts of chalcopyrite, sphalerite, and galena. Late-stage gold-bearing fluids have altered earlier iron and zinc sulfides and have precipitated gold in carbonate-quartz veins. The earliest stage is rep-

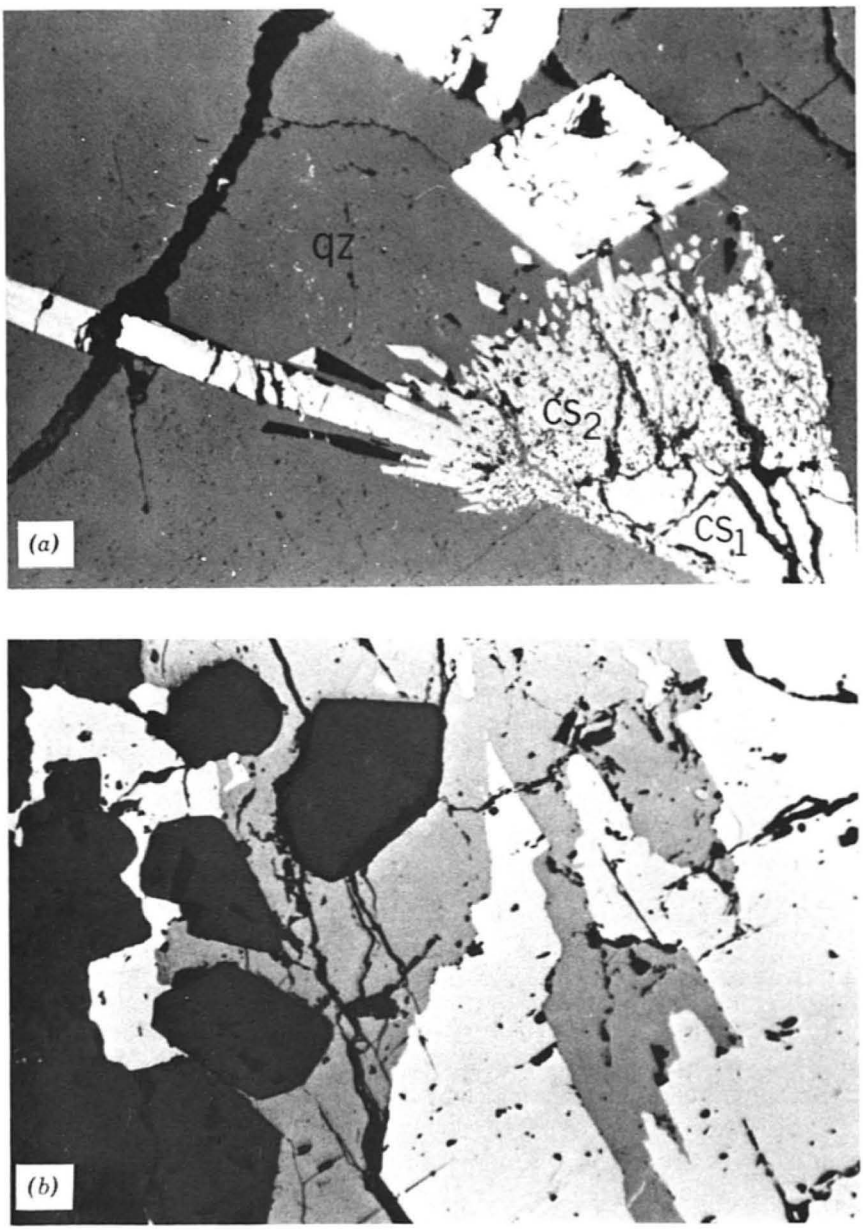

FIGURE 8.11 Tin-tungsten ores from Bolivia illustrating paragenesis of the ore. (*a*) Early cassiterite (cs_1) overgrown by needle-like cassiterite crystals (cs_2). Both generations of cassiterite are enclosed in, and veined by quartz (qz), which also surrounds euhedral pyrite crystals (white); Milluni Mine (width of field = 2,260 μm). (*b*) Early stannite concentrated along contacts of pyrrhotite (white) with older cassiterite (black). The distribution of stannite (gray) is controlled by the basal parting in pyrrhotite; Huanuni Mine (oil immersion, width of field = 1,600 μm). (*c*) Later sulfides (py = pyrite, po = pyrrhotite, sl = sphalerite, cp = chalcopyrite) occurring between grains of

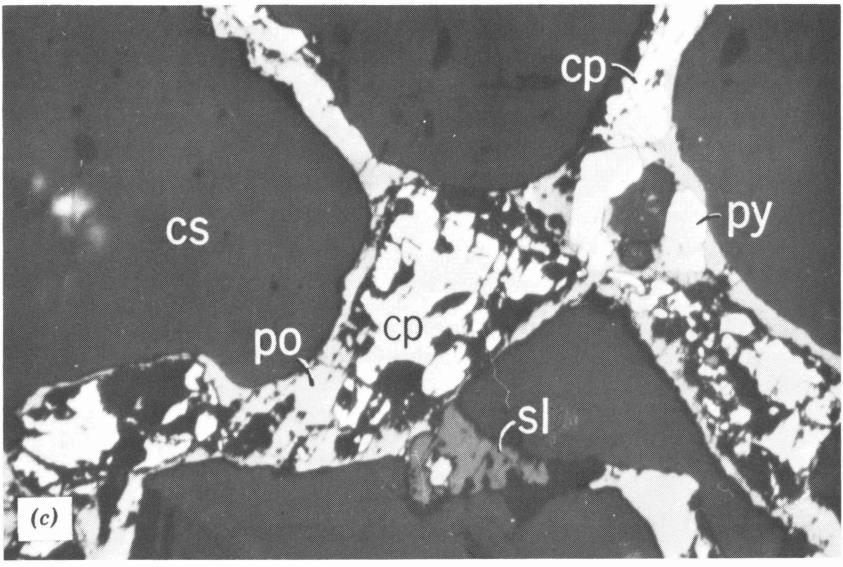

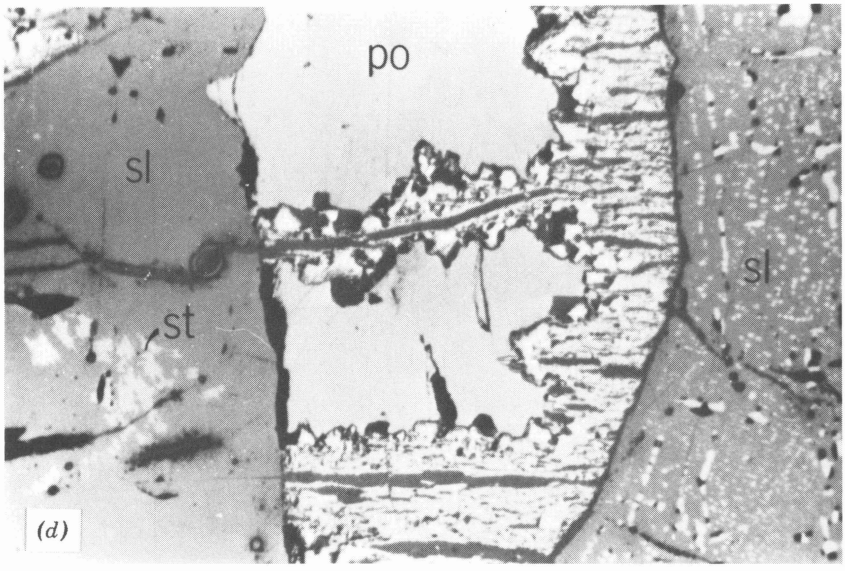

cassiterite (dark gray), Araca Mine (oil immersion, width of field = 960 μm). (*d*) Pyrrhotite (po) containing lamellar intergrowths of pyrite, marcasite, and siderite developed along the contact with early sphalerite (sl) to the right, which contains pyrrhotite and chalcopyrite blebs. Sphalerite to the left contains exsolved stannite (st); Colquiri Mine (width of field = 1,450 μm). (Reproduced from W. C. Kelly and F. S. Turneaure, *Econ. Geol.* **65**, 616, 620, 1970, with permission of the authors and the publisher.)

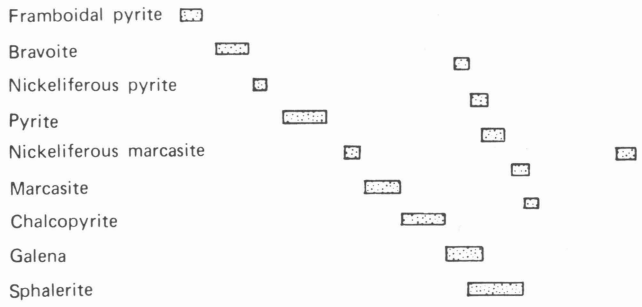

FIGURE 8.12 Diagram illustrating the generalized paragenesis of the ore minerals in the Askrigg Block Area of the North Pennine Orefield, England. (After Vaughan and Ixer, 1980.)

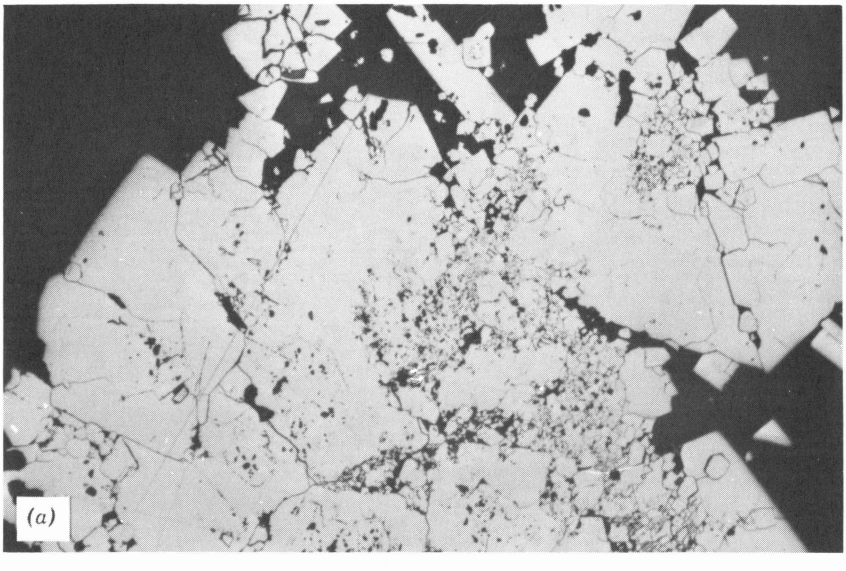

FIGURE 8.13 Sulfide mineral assemblages in the lead-zinc ores of the North Pennines, England, illustrating the paragenesis of the ores. (*a*) Framboidal pyrite overgrown by later euhedral pyrite (oil immersion, width of field = 500 μm). (*b*) Bravoite with overgrowths of later pyrite in a veinlet surrounded by carbonates (oil immersion, width of field = 500 μm). (*c*) Pyrite with associated marcasite (oil immersion and partly crossed polars, width of field = 500 μm). (*d*) Subhedral pyrite grains associated with carbonates and bladed crystals of barite enclosed in later galena (width of field = 500 μm).

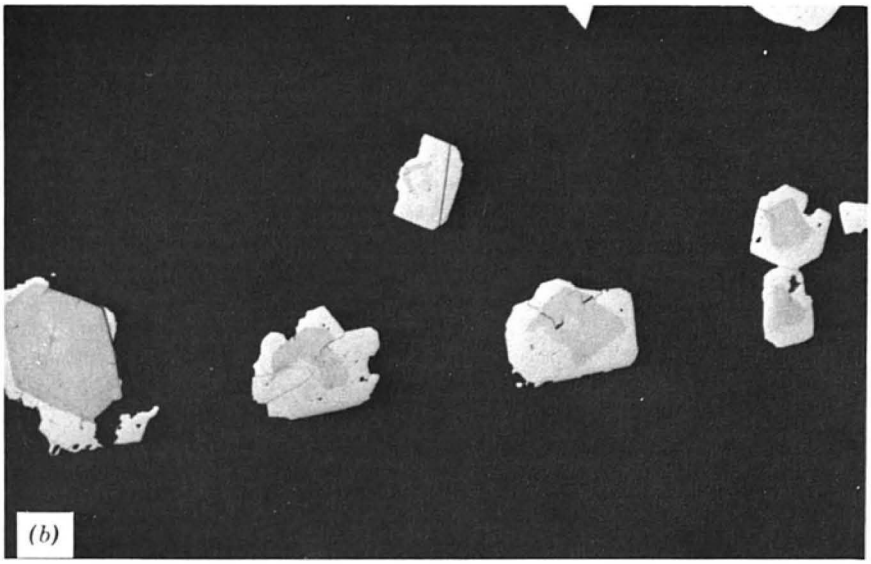
(b)

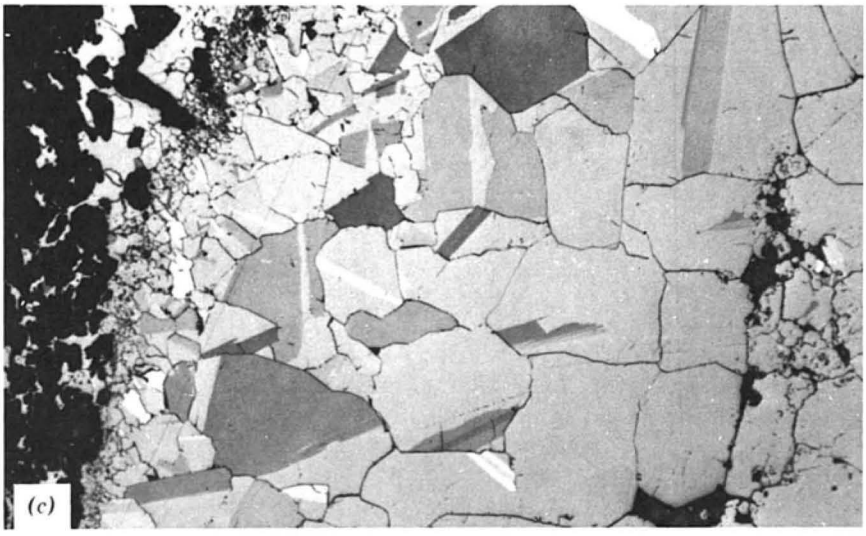
(c)

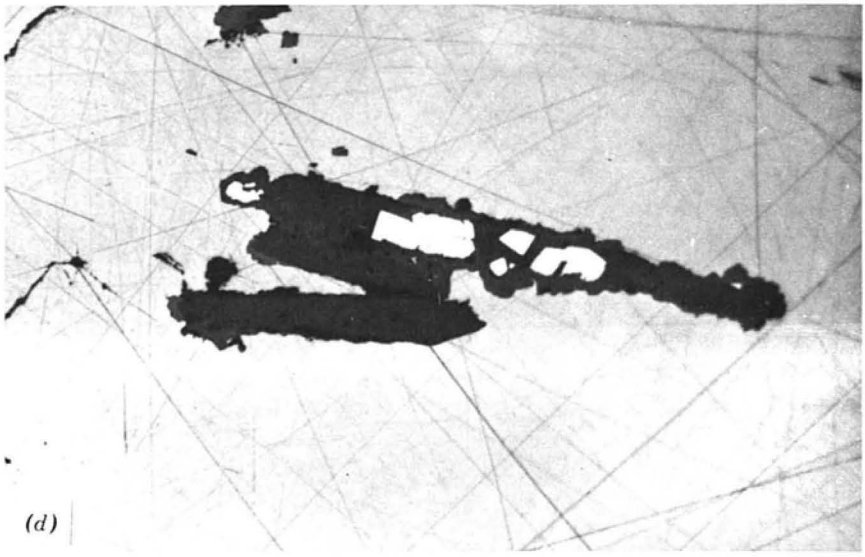
(d)

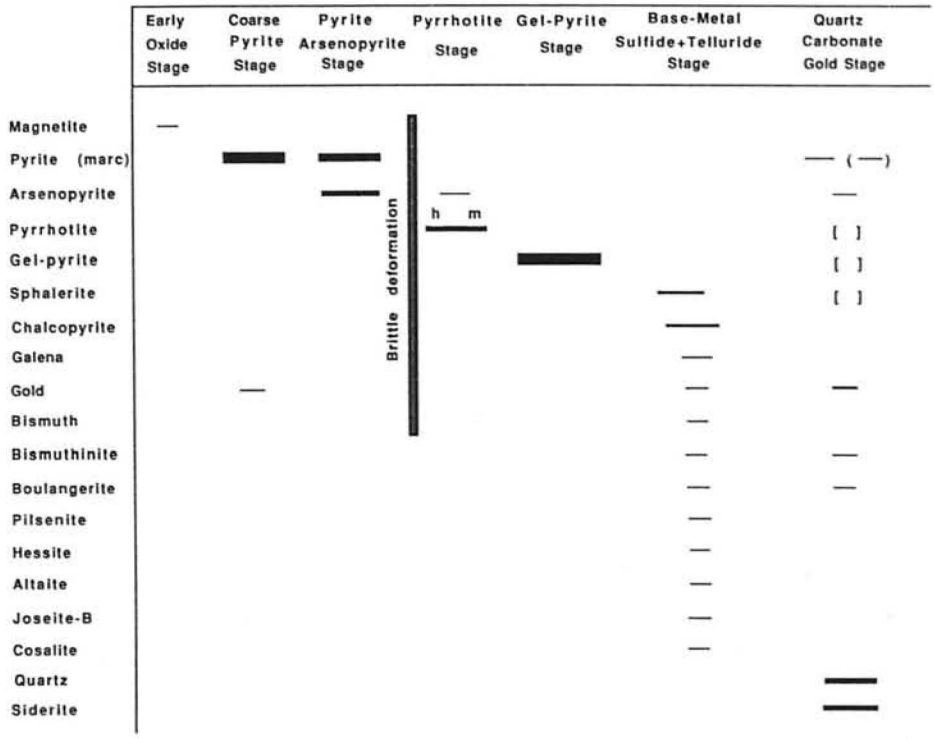

FIGURE 8.14 Figure summarizing the paragenesis of ore mineralization stages of the Mashan deposits of Anhui Province, China. In the diagram, h and m indicate hexagonal and monoclinic pyrrhotite. The brackets in the last stage indicate that the phases already present were modified by the fluids.

resented by local occurrences of magnetite. The coarse pyrite stage is characterized by the presence of pyrite crystals ranging from 1 to 10 cm in diameter; these may contain rare, isolated inclusions of gold. The pyrite-arsenopyrite stage consists of coarsely intergrown pyrite and arsenopyrite, and subhedral to euhedral pyrite that exhibits concentric growth zones defined by different abundances of inclusions. This stage was followed by a period of brittle deformation that locally produced cataclastic textures, as shown in Figure 8.15a.

The "gel pyrite" stage, which is volumetrically the most important stage, is represented by concentrically banded colloform masses of intimately intergrown pyrite and quartz (Figure 8.15b). The gel pyrite occurs in several forms, ranging from a matrix for coarse pyrite crystals to thin veinlets interstitial to crushed pyrite and arsenopyrite. The base metal sulfide and telluride stage is present as masses and grains of chalcopyrite, sphalerite, and galena, interstitial to crystals and fragments of earlier stages. The sphalerite commonly displays "chalcopyrite disease," and the galena locally contains inclusions of silver, lead, and bismuth tellurides (Figure 8.15c). The final stage of ore formation, the quartz-carbonate-gold stage, is evidenced by thin quartz and siderite

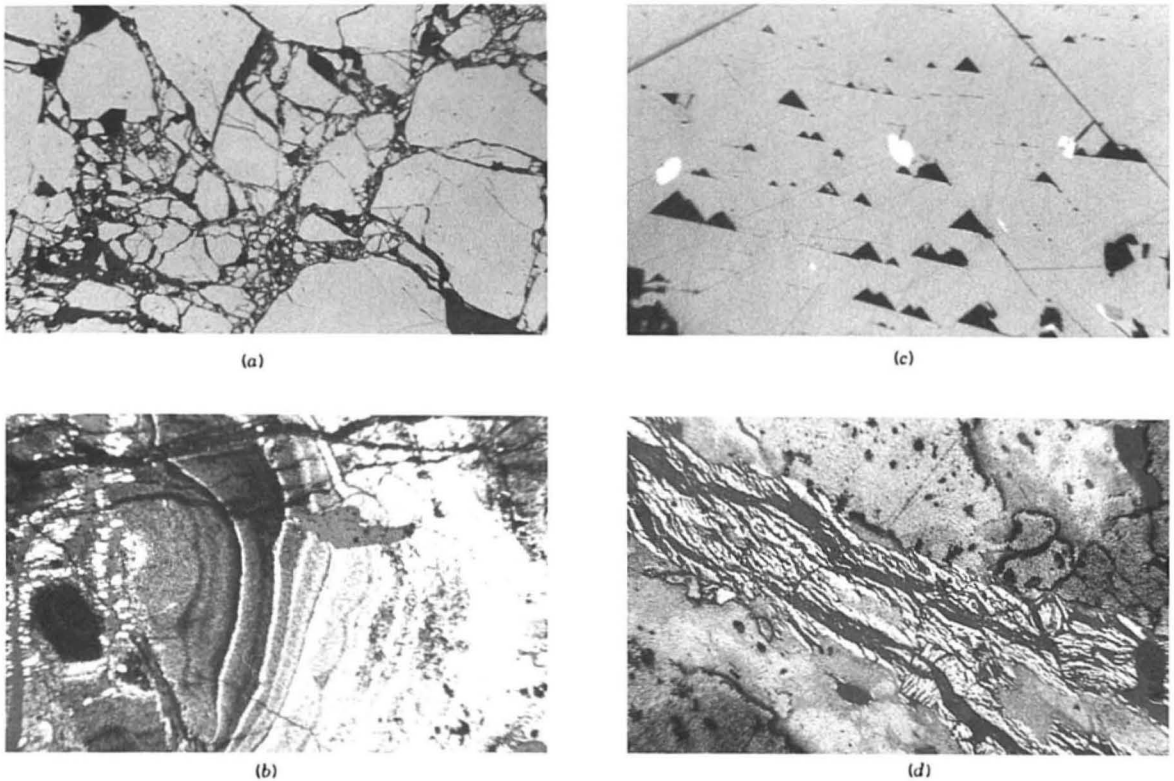

FIGURE 8.15 Gold-bearing base-metal sulfide ores of the Mashan District of Anhui Province, China: (*a*) cataclastically deformed pyrite and arsenopyrite (width of field = 1,200 μm); (*b*) colloform banding of the gel pyrite consists of layers of pyrite, marcasite, and quartz (width of field = 1,200 μm); (*c*) scattered grains of altaite (PbTe, white) and hessite (Ag_2Te, gray) occur within galena (width of field = 600 μm); (*d*) crosscutting veinlets where late fluids have recrystallized gel pyrite into pyrite and marcasite and have deposited small grains of gold (left center) width of field = 1,200 μm).

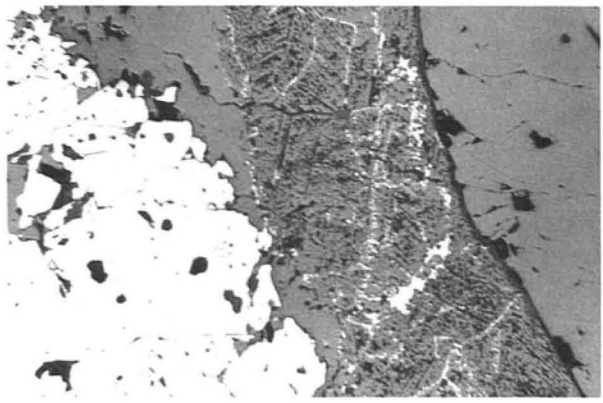

FIGURE 8.16 Late hydrothermal fluids have altered sphalerite in a narrow zone between unaltered iron-rich (7 wt % Fe) sphalerite on the left and pyrite on the right. The oxidizing fluids resulted in raising the activity of sulfur such that iron was removed from the sphalerite, leaving it iron-poor (0.5 wt % Fe) and precipitating the iron as thin veinlets of pyrite and marcasite, Mashan, China (width of field = 1,200 μm).

veinlets that crosscut the earlier stages of mineralization. The mineralizing fluids precipitated small grains of gold (Figure 8.15d) in, and adjacent to, the veinlets and caused recrystallization of the gel pyrite and pyrrhotite to form pyrite and marcasite. The fluids also locally altered the sphalerite by raising the sulfur activity, thus forcing the iron out of the structure as delicate veinlets of pyrite and marcasite (Figure 8.16).

8.4 ORE FORMATION CONDITIONS AND THE APPLICATION OF PHASE EQUILIBRIA DATA

Reference to relevant phase diagrams can help in (1) anticipation and recognition of phases; (2) recognition of trends in ore chemistry (i.e., the character of the ore fluid and its variation in time or space); (3) understanding of reactions and some textural features (e.g., exsolution); (4) understanding of the correlation or antipathetic relationships between phases; (5) recognition of equilibrium or disequilibrium mineral assemblages; (6) interpretation of the nature of the ore-forming fluid and the mechanisms that were operable during mineralization; and (6) estimation of the temperature and pressure during ore formation or subsequent metamorphism.

It is impossible to present more than a few of the many relevant phase diagrams, but the following systems are discussed, at least in part, in this book:

Fe-S	Figure 8.18
Cu-S	Figure 10.8
Cu-Fe-S	Figure 7.14 and 8.17

Fe-Ni-S	Figures 9.6 and 9.7
Fe-Zn-S	Figure 10.28
Fe-As-S	Figure 8.19
FeO-Fe_2O_3-TiO_2	Figures 9.12 and 9.13
Cr_2O_3-$(Mg,Fe)O$-SiO_2	Figure 9.4
Au-Ag-Te	Figure 9.25
Ca-Fe-Si-C-O	Figure 10.31
Cu-O-H-S-Cl	Figure 10.11
U-O_2-CO_2-H_2O	Figure 10.9
NaCl-KCl-H_2O	Figure 8.24
H_2O(P-T)	Figure 8.25
Iron Minerals (Eh-pH)	Figure 10.3

For additional information on these and other systems, the reader is referred to *Mineral Chemistry of Metal Sulfides* (Vaughan and Craig, 1978), "Sulfide Phase Equilibria" (Barton and Skinner) in *Geochemistry of Hydrothermal Ore Deposits* (1979), *Sulphide Minerals: Crystal Chemistry Paragenesis and Systematics* (Kostov and Mincheeva-Stefanova, 1981), *Sulfide Minerals* (Ribbe, 1974), and *Oxide Minerals* (Rumble, 1976; Lindsley, 1991). Most diagrams in the literature are "equilibrium" diagrams and may be cautiously applied to the natural ores, which also represent, at least locally, conditions of equilibrium. For example, in Cu-Fe-sulfide ores, assemblages such as pyrite-pyrrhotite-chalcopyrite, pyrite-chalcopyrite-bornite, or even pyrite-digenite-bornite are common, because they are stable (see Figure 8.17), whereas pyrrhotite-covellite or cubanite-chalcocite assemblages are unknown and are not expected, because they are not stable. It is important to note that, although most ore mineral assemblages do represent equilibrium, disequilibrium assemblages are not uncommon. This is especially true in weathering zones in which reaction kinetics are slow because of the low temperatures involved.

Phase diagrams are important in providing geothermometric and geobarometric data. The geothermometers are of two types—*sliding scale* and *fixed point*. The sliding-scale type is based on the temperature dependence of the composition of a mineral or a pair of minerals when it is part of a specified assemblage (e.g., the composition of pyrrhotite in equilibrium with pyrite in Figure 8.18a). Ideally, determination of the composition of pyrrhotite coexisting with pyrite would uniquely define the temperature of equilibration; in practice, however, it has been found that nearly all pyrrhotites have re-equilibrated during cooling, some to near room temperature conditions (see Figure 8.18b). Unfortunately, the rapid rates of sulfide re-equilibration processes have limited the usefulness of many sliding-scale geothermometers. Two notable exceptions involve refractory minerals that retain their high-temperature compositions during cooling and thus are applicable as sliding-scale geothermometers, namely,

1. Arsenopyrite when equilibrated with pyrite and pyrrhotite (and some other less common assemblages), as shown in Figure 8.19.

2. Coexisting magnetite-ulvöspinel and ilmenite-hematite. The compositions of these minerals, if equilibrated together, uniquely define both the temperature and the oxygen activity of equilibration, as shown in Figure 9.13.

Fixed-point geothermometers are minerals or mineral assemblages that undergo a reaction (e.g., melting, inversion, reaction to form a different assemblage) at a defined temperature. For example, crystals of stibnite must have formed below its melting point (556°C), and the mineral pair pyrite plus arsenopyrite must have formed below 491°C. The fixed points thus do not

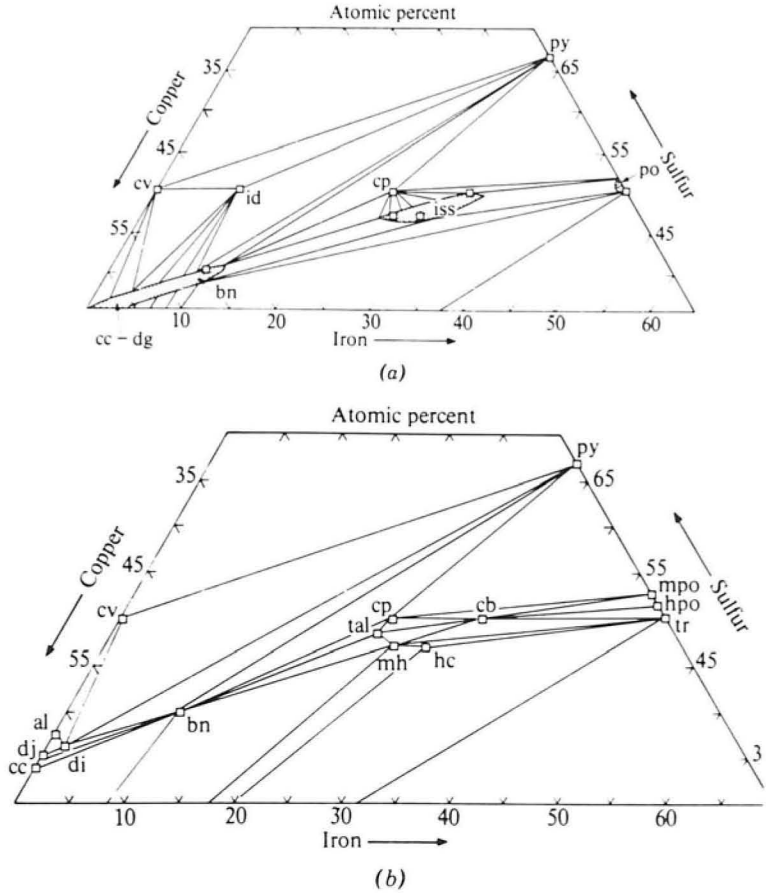

FIGURE 8.17 Phase relations in the central portion of the Cu-Fe-S system: (*a*) schematic relations at 300°C; (*b*) possible phase relations at 25°C. Abbreviations are as follows: cc, chalcocite; dj, djurleite; di, digenite; al, anilite; cv, covellite; bn, bornite; id, idaite; cp, chalcopyrite; tal, talnakhite; mh, mooihoekite; hc, haycockite; cb, cubanite; mpo, monoclinic pyrrhotite; hpo, hexagonal pyrrhotite; tr, troilite; py, pyrite; iss, intermediate solid solution. (From Vaughan and Craig, 1978; used with permission.)

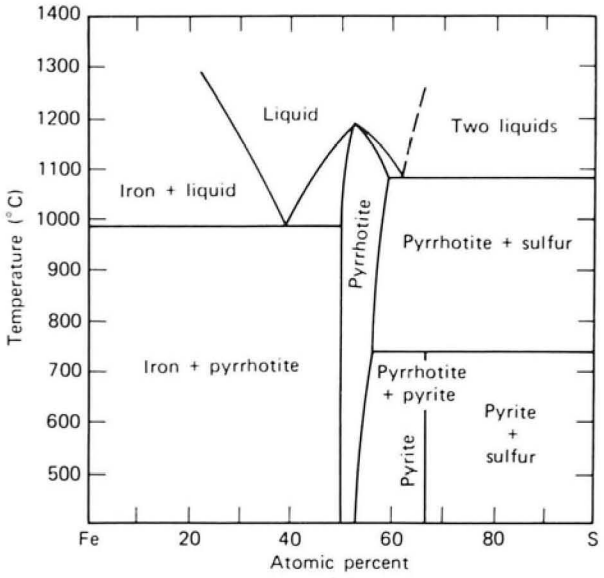

(*a*)

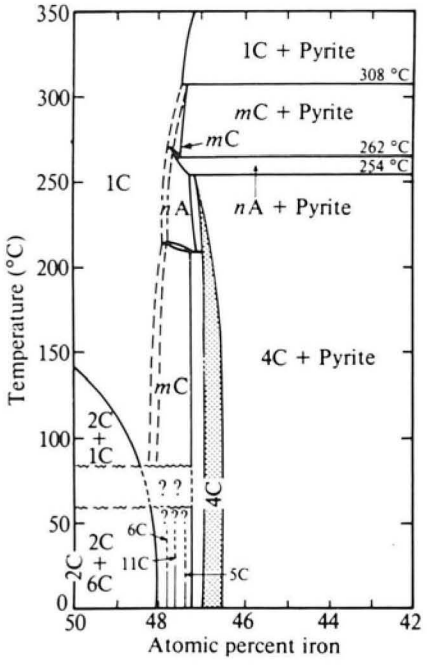

(*b*)

FIGURE 8.18 Phase relations among condensed phases in the Fe-S system: (*a*) above 400°C; (*b*) in the central portion of the system below 350°C. The notations 2C, 1C, 6C, 4C, 11C, and mC refer to c-axis superstructure dimensions, and nA to a-axis superstructure dimensions in pyrrhotites. (From Vaughan and Craig, 1978; used with permission.)

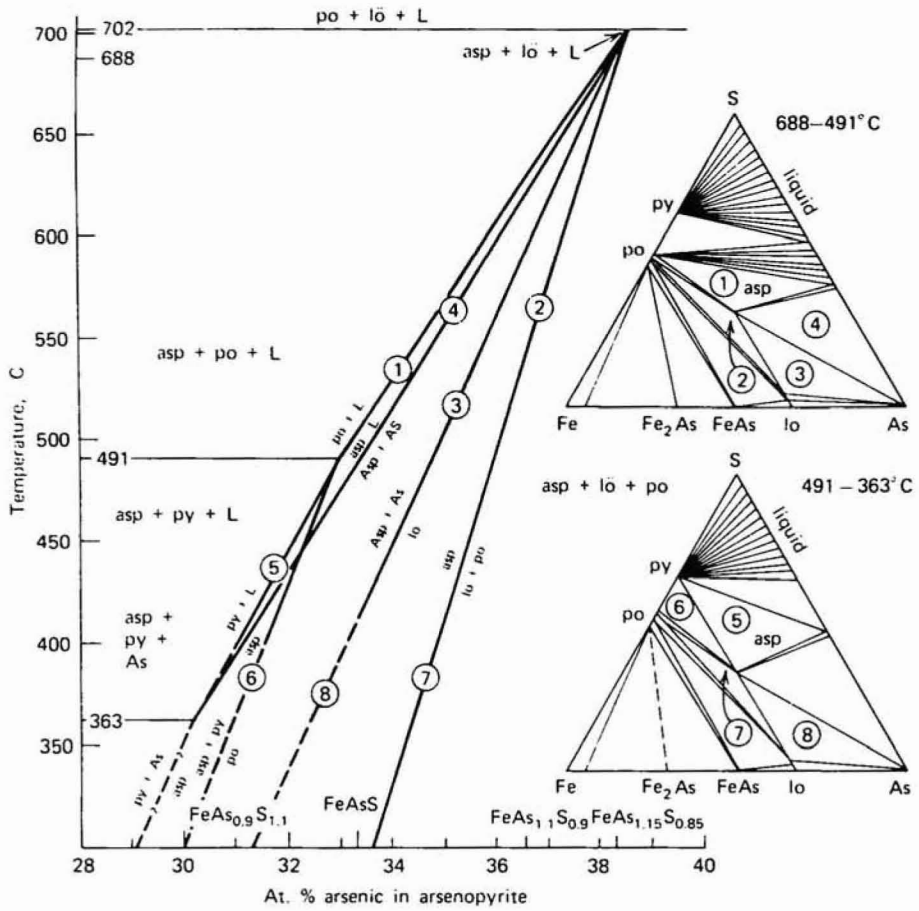

FIGURE 8.19 Pseudobinary temperature—composition plot showing arsenopyrite composition as a function of temperature and equilibrium mineral assemblage. The assemblages numbered 1–8 in the Fe-As-S phase diagrams on the right correspond to the labeled curves in the diagram on the left. Abbreviations are as follows: asp, arsenopyrite; py, pyrite; po, pyrrhotite; lö, löllingite; L, liquid. (After U. Kretschmar and S. D. Scott, *Can. Mineral.* **14**, 366–372, 1976; used with permission.)

sharply define the temperature of equilibration but rather set upper and lower limits. Barton and Skinner (1979) and Vaughan and Craig (1978) have prepared extensive lists of reaction points that serve as potentially useful fixed-point geothermometers. Most fixed points are known only for very low pressures; those whose pressure dependence has been determined generally rise at a rate of about 10°C kbar.

Phase equilibria studies have revealed that the iron content of sphalerite equilibrated with pyrite and pyrrhotite, although temperature independent between about 300° and 550°, is pressure dependent. This relationship has been defined (Scott and Barnes, 1971; Scott, 1973; Lusk and Ford, 1978) and

thus allows the sphalerite composition in this assemblage to serve as a geobarometer (Figure 10.28). The following equation relates iron content (as FeS) to the pressure of equilibration (Hutchison and Scott, 1981):

$$P \text{ bar} = 42.30 - 32.10 \log \text{mole \% FeS}$$

Although sphalerite is among the most refractory of ore minerals and thus may preserve a composition indicative of the original pressure of equilibration with pyrite and pyrrhotite, sphalerite often undergoes at least partial re-equilibration (Barton and Skinner, 1979). Such re-equilibration, which is most evident where the sphalerite is in contact with pyrrhotite or chalcopyrite, results in a decrease in the FeS content of the sphalerite. Consequently, Hutchison and Scott (1979) and Brooker, Craig, and Rimstidt (1987) found that sphalerite inclusions that equilibrated with pyrite and pyrrhotite in metamorphosed ores and that were trapped within recrystallizing pyrite seemed to preserve compositions that best reflected the metamorphic pressures. When partial re-equilibration of sphalerite has occurred, those with highest FeS contents are probably most indicative of the pressures of original equilibration, because lower-temperature re-equilibration reduces the FeS content.

8.5 FLUID INCLUSION STUDIES

The study of fluid inclusions, although commonly carried out on nonopaque minerals using a transmitted-light microscope, has become a major and important field of investigation that is commonly carried out simultaneously with conventional ore microscopy to provide vital information about the fluids associated with ore formation. In particular, it provides valuable data on the temperatures and pressures of ore formation or subsequent metamorphism and on the chemistry of the ore fluids. Fluid inclusions are abundant in many common ore and gangue minerals and can be observed with a standard petrographic microscope. Accordingly, a brief discussion of the nature and significance of fluid inclusions and the means of preparing samples for their study is presented in the following subsections for more detailed descriptions, the reader is referred to Cunningham (1976), Roedder (1979, 1984), and Shepherd, Rankin and Alderton (1985) and the other references presented at the end of this chapter.

8.5.1 The Nature and Location of Fluid Inclusions

Fluid inclusions are small amounts of fluid that are trapped within crystals during initial growth from solution or during total recrystallization (*primary inclusions*) or during localized recrystallization along fractures at some later time (*secondary inclusions*). Fluid inclusions are very abundant in common ore

and gangue minerals, sometimes occurring in quantities of a billion or more per cubic centimeter. Their volumes are often less than 10 μm^3 but may reach as much as a cubic millimeter or more. However, despite their widespread occurrence and abundance, fluid inclusions are seldom recognized in conventional polished sections, because so little light actually enters most ore minerals; even among the most transparent of ore minerals, inclusions are rarely recognized as anything except internal reflections. However, when transparent ore and gangue minerals are properly prepared and observed in transmitted light, as described later, they are often found to contain abundant tiny inclusions, commonly oriented along well-defined crystallographic planes (Figure 8.20) and having a wide variety of shapes. Some inclusions (Figure 8.21) may contain visible bubbles or mineral grains that precipitated at the time of trapping or that precipitated from the fluid after trapping (daughter minerals).

Primary inclusions, those trapped during growth of the host mineral, may be samples of the ore-forming fluid and may reveal important information regarding the conditions of ore transport and deposition. Bodnar and Sterner (1987), as well as several subsequent studies, have demonstrated through the development of synthetic fluid inclusions that the fluids do, in fact, reveal accurate information on entrapment conditions. Roedder (pers. commun., 1980), however, has pointed out that there has been alternation of ore and gangue mineral deposition in many ores without simultaneous deposition. If this has occurred, fluid inclusions in gangue minerals may not represent the fluids from which the ore minerals formed.

Secondary inclusions must be used with care, because they represent fluids passing through the rocks after the crystallization of the minerals in which these inclusions are found. Accordingly, they may contain fluids from a later stage of ore formation, a postore fluid related to the ore-forming episode, a metamorphic fluid, or even a late deuteric alteration or weathering fluid. If their position in the paragenesis can be established, they may still provide valuable information on the ore-forming process. Unfortunately, the distinction between primary and secondary inclusions is often not unequivocal. Roedder (1984) has offered the empirical criteria listed in Table 8.1 to help in interpretation; clearly, understanding the paragenesis of an ore, as discussed in the beginning of this chapter, helps in the interpretation of fluid inclusions, and vice versa. The reader is directed to Roedder's book for additional discussion.

Commonly, the fluids trapped along growing crystal faces are homogeneous; however, sometimes two or more immiscible liquids (i.e., water and oil or water and CO_2), liquids and gases (i.e., boiling water and steam), or liquids plus solids (i.e., water plus salts or other minerals) may be trapped together. Such inclusions (termed multiphase inclusions) are difficult to interpret geothermometrically but may provide considerable data on the nature of the ore-forming fluid. Typical host minerals in which fluid inclusions are observed include sphalerite, cassiterite, quartz, calcite, dolomite, fluorite, and

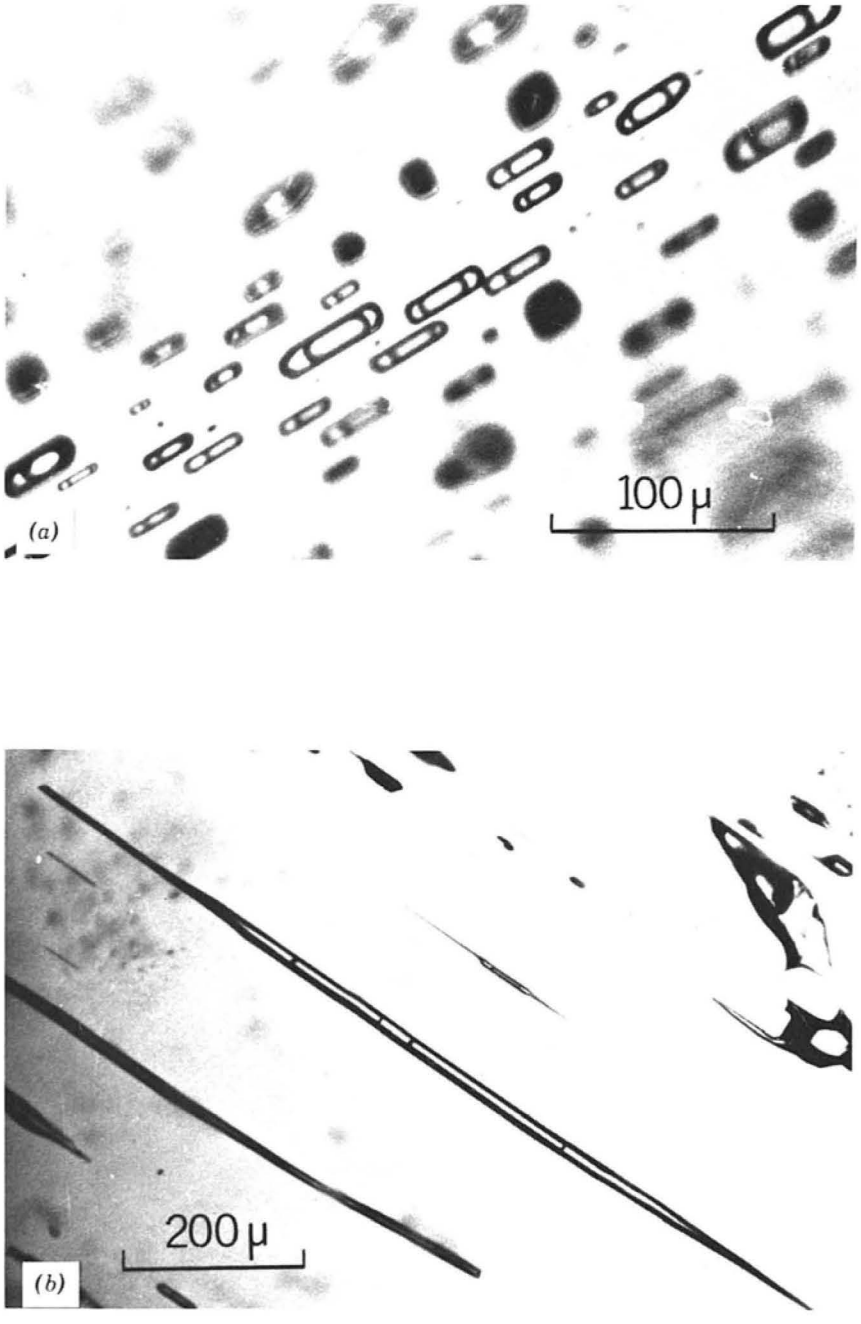

FIGURE 8.20 Fluid inclusions in cassiterite, Oruro District, Bolivia. (*a*) Inclusions lying along a healed cleavage plane. The gas phase fills the inclusions at 424–434°C. (*b*) Needle-like inclusions, some with double bubbles due to constriction of the chamber. (Reproduced from W. C. Kelly and F. S. Turneaure, *Econ. Geol.* **65**, 649, 1970, with permission of the authors and the publisher.)

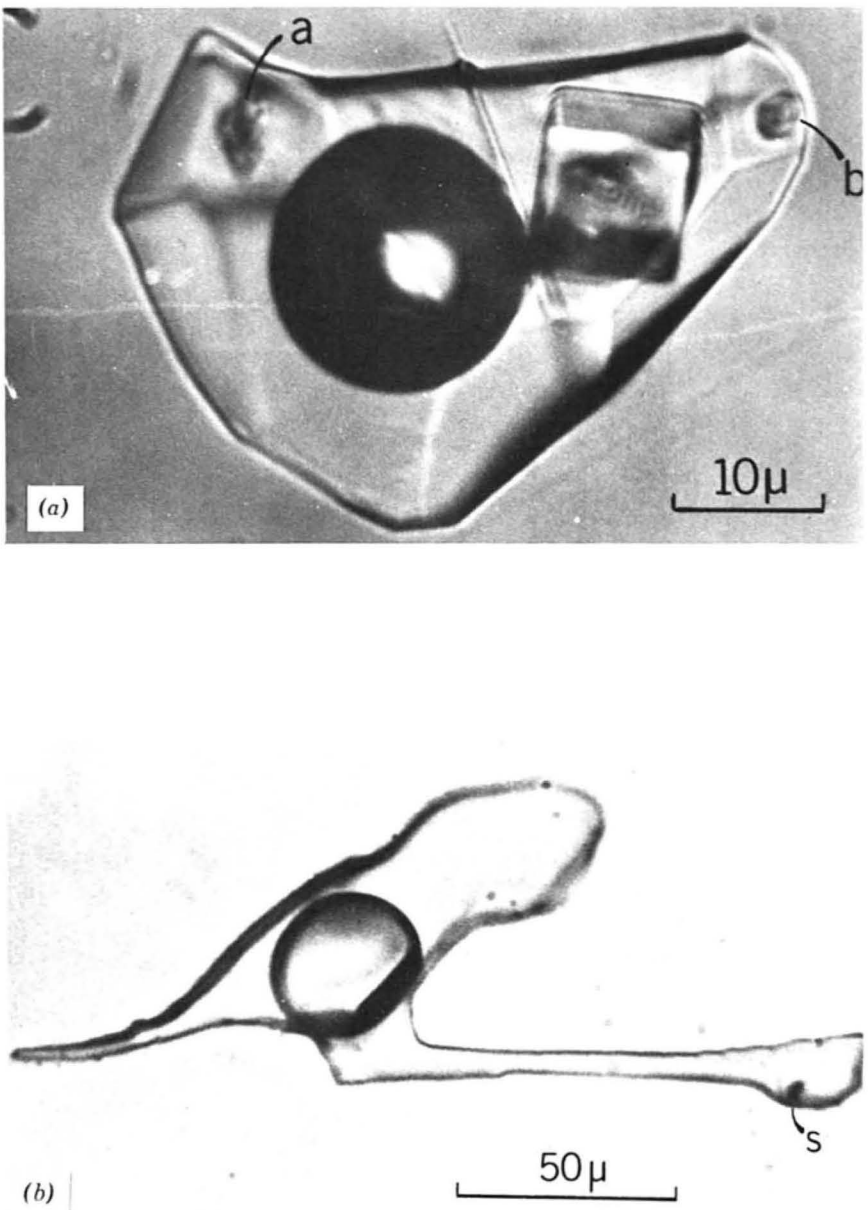

FIGURE 8.21 Fluid inclusions that contain daughter inclusions. (*a*) Inclusion in quartz, with a large halite cube and unidentified daughter salts at *a* and *b*. The total salinity is approximately 47%, and the fluid fills the inclusion at 430°C; Gigante Chica, Laramcota Mine, Bolivia. (*b*) Inclusion in apatite having an irregular form suggestive of necking down. A grain of an opaque inclusion at *s* lies in front of a small halite cube. The inclusion fills with liquid at 350°C; Lallaqua Mine, Bolivia. (Reproduced from W. C. Kelly and F. C. Turneaure, *Econ. Geol.* **65**, 651, 1970, with permission of the authors and the publisher.)

TABLE 8.1 Criteria for Recognition of the Origin of Fluid Inclusions (revised from Roedder 1976, 1979)

Criteria for Primary Origin

Single crystals with or without evidence of direction of growth or growth zonation.
- Occurrence as a single inclusion (or isolated group) in an otherwise inclusion-free crystal
- Large size of inclusion(s) relative to enclosing crystal (e.g., 1/10 of crystal) and of equant shape
- Isolated occurrence of inclusion away from other inclusions (e.g., $\geqslant$ inclusion diameters)
- Random three-dimensional occurrence of inclusions in crystal
- Occurrence of daughter minerals of the same type as occur as solid inclusions in the host crystal or contemporaneous phases

Single Crystals Showing Evidence of Directional Growth

Occurrence of inclusion along boundary between two different stages of growth (e.g. contact between zone of inimpeded growth and zone containing extraneous solid inclusions)

Occurrence of inclusion in a growth zone beyond a visibly healed crack in earlier growth stages

Occurrence of inclusion at boundary between subparallel growth zones

Occurrence of inclusion at intersection of growth spirals

Occurrence of relatively large flat inclusions in the core or parallel to external crystal faces

Occurrence of inclusion(s) at the intersection of two crystal faces

Single Crystals Showing Evidence of Growth Zonation (on the Basis of Color, Solid Inclusions, Clarity, etc.)

Occurrence of different frequencies or morphologies of fluid inclusions in adjacent growth zones

Occurrence of planar arrays outlining growth zones (unless parallel to cleavage directions)

Crystals Evidencing Growth from Heterogeneous (i.e., Two-Phase) or Changing Fluid

Occurrence of inclusions with differing contents in adjacent growth layers (e.g., gas inclusions in one layer, liquid in another layer, or oil and water in another layer, etc.)

Occurrence of inclusions containing some growth medium at points where host crystal has overgrown and surrounded adhering globules of an immiscible phase (e.g., oil droplets)

Occurrence of primary-appearing inclusions with "unlikely" growth medium (e.g., mercury in calcite, oil in fluorite or calcite, etc.)

Hosts Other Than Single Crystals

Occurrence of inclusions at growth surfaces of nonparallel crystals (these have often leaked and could be secondary)

TABLE 8.1 (*Continued*)

Occurrence of inclusions in polycrystalline hosts (e.g., vesicles in basalt, fine-grained dolomite, vugs in pegmatites—these have usually leaked)
Occurrence in noncrystalline hosts (e.g., bubbles in amber, vesicles in pumice)
Criteria for Secondary Origin
Occurrence of inclusions in planar groups along planes that crosscut crystals or that parallel cleavages
Occurrence of very thin, flat, or obviously "necking-down" inclusions
Occurrence of primary inclusions with filling representative of secondary conditions
Occurrence of inclusions along a healed fracture
Occurrence of empty inclusions in portions of crystals where all other inclusions are filled
Occurrence of inclusions that exhibit much lower (or, more rarely, higher) filling temperatures than adjacent inclusions
Criteria for Pseudosecondary Origin
Occurrence of secondary-like inclusions with a fracture visibly terminating within a crystal
Occurrence of equant and negative crystal-shaped inclusions
Occurrence of inclusions in etch pits crosscutting growth zones

barite, but nearly any transparent mineral may contain visible inclusions. Roedder (1979) even notes that some granite feldspars contain so many fluid inclusions with daughter NaCl crystals that NaCl diffraction lines appear in single-crystal X-ray photographs of the feldspars. The opaque ore minerals such as galena and pyrite contain inclusions, the forms of which may be seen on some fractured or cleaved surfaces, but present techniques do not permit their undisturbed in situ observation. There has been some successful application of light sources employing light of wavelengths outside the visible spectrum to examine inclusions in opaque materials, and such techniques will probably prove to be useful in the future.

8.5.2 Changes in Fluid Inclusions Since Trapping

Most fluid inclusions were trapped as a homogeneous fluid at elevated temperatures and pressures. During the subsequent cooling, the fluid may have separated into liquid and vapor, because the fluid contracts much more than the solid host mineral. Immiscible fluids may separate on cooling, and daughter crystals, usually halite or sylvite, may precipitate as saturation of the fluid occurs. Many inclusions do not now have the shape they originally possessed because of solution and deposition in different parts of the inclusion cavity. In general, inclusions will tend, by solution and redeposition, to

reduce surface area and to become more equant. Through this process, elongate inclusions may separate into several more equant inclusions as a result of "necking down," as shown in Figure 8.22. If the necking down occurs after phase separation, the process may isolate the vapor bubble in one of the new inclusions while leaving another new inclusion completely fluid filled. As a result, neither inclusion would be representative of the originally trapped fluid, and the information that could be derived would be limited. Larger flat primary inclusions or secondary cracks may also undergo considerable recrystallization (Figure 8.23), in which one large inclusion is reduced to many small ones occupying the same region within the crystal. Roedder (1977) has cautioned the student of fluid inclusions as follows: "It is important to remember always that the fluid inclusions in a mineral provide information only on the fluids present *at the time of sealing* of the inclusion, whether that be during the growth of the host crystal or during rehealing of a later fracture."

Leakage, the movement of material into or out of the original inclusion, can occur but is not common; one exception may be high-grade metamorphism in which re-equilibration can markedly alter inclusions. It is evident, however, when one observes planes containing large numbers of inclusions, all of which are empty. In general, quartz, fluorite, calcite, and sphalerite are free from leakage problems; barite and gypsum are more prone to such problems.

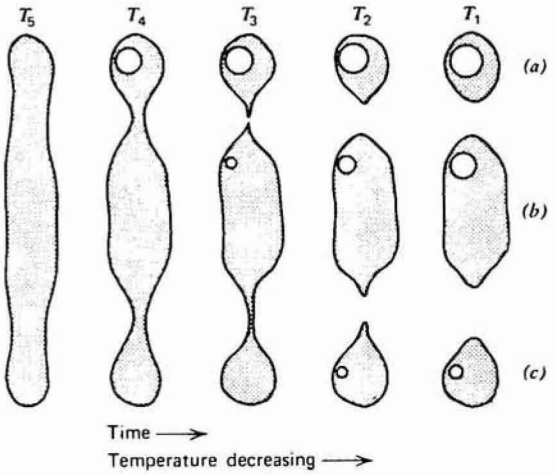

FIGURE 8.22 Necking down of a long tubular inclusion. The original inclusion, trapped at temperature T_5, breaks up during slow cooling to form three separate inclusions, *a*, *b*, and *c*. Upon reheating in the laboratory, inclusion *a* would homogenize above the true trapping temperature T_5, inclusion *b* would homogenize above T_5, and inclusion *c* would homogenize between T_3 and T_3. (Reproduced from E. Roedder, in *Geochemistry of Hydrothermal Ore Deposits*, 2nd ed., copyright © 1979, Wiley Interscience, New York p. 903, with permission of the publisher.)

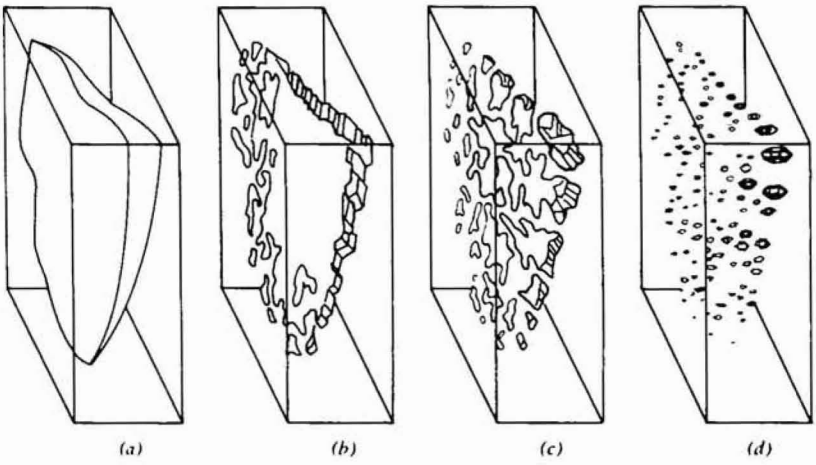

FIGURE 8.23 Healing of a crack in a quartz crystal, resulting in secondary inclusions. Solution of some of the curved surfaces having nonrational indices and redeposition as dendrite crystal growth on others eventually result in the formation of sharpy faceted negative crystal inclusions. If this process occurs with falling temperature, the individual inclusions will have a variety of gas-liquid ratios. (Reproduced from E. Roedder in Ceochemistry of Hydrothermal Ore Deposits, 2nd ed., copyright © 1979, Wiley Interscience, New York p. 702, with permission of the publisher.)

8.5.3 The Preparation of Samples and the Observation of Fluid Inclusions

Fluid inclusions commonly go unnoticed, both because the observer is not looking for them and because conventional polished sections and thin sections are poorly suited for their observation. Fluid inclusions are best seen and studied in small single crystals, cleavage fragments, or cut mineral plates that are thick enough to contain the undamaged inclusion but thin enough to readily transmit light, and that are doubly polished to minimize the interferences of surface imperfections and excessive diffuse light scattering; details are described in Brumby and Shepherd (1978) and Roedder (1984) and a flow chart of preparation steps is given in Figure 2.8. The ideal sample thickness varies from one specimen to another, depending on the transparency, the grain size, and the size of the inclusions; for most samples, 0.5–1.0 mm is quite satisfactory. Some crystals or granular aggregates can be cut directly, but many need support and are best cut after having been cast in a polyester resin. The polyester is readily dissolved in chloroform; thus, the sample plate can be removed after cutting and polishing have been completed. The polyester block with enclosed sample is cut into one or more 1.0–1.5 mm thick plates. High-speed diamond saws may induce considerable fracturing in specimens and should not be used to cut samples for fluid inclusion studies; slow-speed, thin-blade diamond saws give clean cuts with minimal sample damage. Polishing of the plates is often facilitated by bonding them to a supporting

aluminum, brass, or glass disk with a low melting-point resin (such as Lakeside Type 30C), or a soluble glue (such as super glue, soluble in acetone). After one side is polished, the plate is released from the supporting metal disk, turned over, and readhered so that the other side may be similarly polished. When polishing is completed, the plate is released from the support disk, the polyester is removed, and the plate is ready for examination. It is important to remember that these adhesives and their solvents may contain chemicals that are flammable and that are harmful if inhaled. Hence, they should be used with care and in a fume hood.

Fluid inclusions range in size from rare megascopically visible examples that are greater than 1 cm in length to submicroscopic examples; most work has, however, been carried out on those that range upward from 10 μm. Inclusions of 10 μm or larger are readily observed within small crystals, cleavage fragments, or polished plates by examination using a standard microscope. Such specimens may be placed on a glass microscope slide and viewed with transmitted light. Care must be taken, however, not to allow high-magnification lenses, which have short free-working distances, to strike the specimen. Since the depth of field is very limited on such lenses, it is easy for the observer to strike the lens on the sample when adjusting focus to follow a plane of inclusions into the sample. Lenses with long free-working distances, such as those designed for use with the universal stage, are very useful and are necessary when using heating and cooling stages. Because bubbles frequently seem to be located in the least visible corner of an inclusion, auxiliary oblique lighting systems are useful. In addition, a colored filter or a monochromatic light source may prove to be useful in seeing the inclusions and daughter phases.

It is obviously important to study inclusions in samples that have been well documented in terms of their mineralogy, location, and paragenesis; measurements of freezing point depression and inclusion homogenization on heating should be made on the same inclusions.

8.5.4 The Compositions of Fluid Inclusions

Fluid inclusions are extremely important in the study of ore deposits, because they often represent unaltered, or at least minimally altered, samples of the ore-forming fluid (see Roedder, 1990 for a review of techniques for fluid inclusion analysis). Most workers do not have facilities to determine the actual chemical composition of the inclusions that they observe, but they can determine the salinity of the trapped solution by measuring the freezing temperature, as described in Section 8.5.5.

The most comprehensive listing of compositional data for fluid inclusions is that by Roedder (1972), but there now exist thousands of papers that contain useful comparative data. By far the most abundant type of inclusion is that which contains a low-viscosity liquid and a smaller-volume gas or vapor bubble. The liquid is generally aqueous, has a pH within one unit of neutral, and

contains a total salt concentration between 0 and 40 wt %. The salts consist of major amounts of Na^+, K^+, Ca^{2+}, Mg^{2+}, Cl^-, and SO_4^{2-}, with minor amounts of Li^+, Al^{3+}, BO_3^{3-}, H_4SiO_4, HCO_3^-, and CO_3^{2-}. Na^+ and Cl^- are usually dominant; carbon dioxide, in both liquid and gas form, and liquid hydrocarbons, are fairly common. Liquid hydrogen sulfide has also been observed, but it is rare. Fluid carbon dioxide will never be observed above 31°C, its critical point; hence, the fluid inclusion observer must be careful of sample heating by the light source and even of working in a hot room. Daughter minerals, usually cubes of halite (NaCl) or sylvite (KCl), form when nearly saturated fluids cool from the initial temperature of entrapment. The presence of such crystals obviously indicates that the fluid is salt saturated. Other crystals that are observed in fluid inclusions but that are not simple precipitates of a supersaturated solution include sulfides, quartz, anhydrite, calcite, hematite, and gypsum. Such crystals probably either formed before the inclusion was finally sealed, as a result of secondarily introduced fluids, or even through oxidation resulting from hydrogen diffusion. For example, $2Fe^{2+}$ (soln.) $3H_2O = Fe_2O_3$ (hematite) + $4H^+ + H_2$ (lost through diffusion).

The total NaCl-equivalent salinity of fluid inclusions can be determined by the freezing-point depression method. In practice, this is achieved by freezing

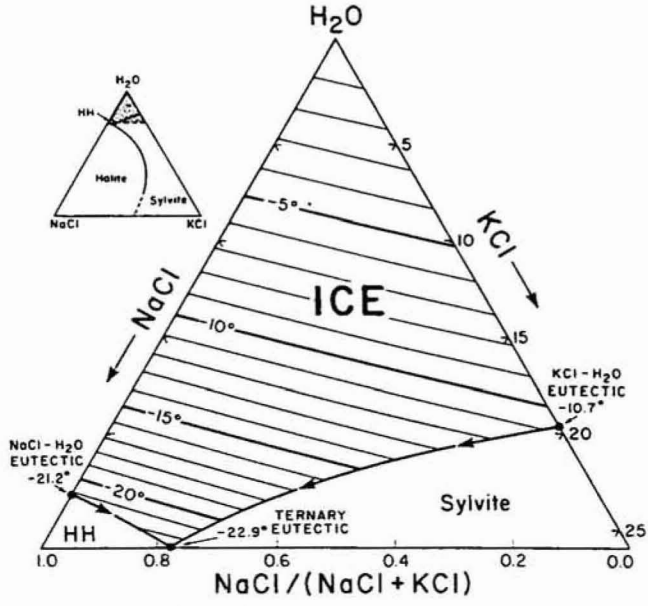

FIGURE 8.24 Isotherms along the vapor-saturated solubility surface within the ice-stable region of the NaCl-KCl-H_2O system. The larger diagram, expressed in weight percent NaCl and KCl, is an enlargement of the shaded portion of the smaller diagram. Salinities measured by observation of ice melting are expressed as NaCl-equivalent, and it is apparent that the presence of small amounts of KCl do not have much effect on the NaCl-H_2O relationships. (Reproduced from Hall et al., 1988, *Econ. Geol.* **83**, 197 with permission.)

the sample, then observing it through the microscope as it is warmed and measuring the temperature at which the last ice melts. This temperature is then used to read off the solution composition from a curve on a diagram, such as Figure 8.24, or calculated from equations such as those prepared by Potter, Clynne, and Brown (1978). The curves represent the freezing-point depression of water as a function of salt content.

Fluid inclusions are cooled or heated by means of stages that mount on a conventional microscope. Commercial designs such as the U.S.G.S. gas flow stage, the Leitz 350, the R. Chaix M.E.C.A. or the Linkham are in common use, as are a wide variety of "homemade" models. In all such fluid inclusion stages, the samples are held and heated or cooled within a chamber that is equipped with a viewing window. Roedder (1976) has pointed out that "the operation of any heating stage must be done with care and constant consideration of the possible sources of error, as it is surprisingly easy to get beautifully consistent, reproducible, but incorrect numbers." Accordingly, prior to use, the stage should be carefully tested for thermal gradients and calibrated with standards. The problems are especially acute in freezing-point determinations, because an error of 1°C is equivalent to an error of about 1 wt % NaCl equivalent.

8.5.5 Fluid Inclusion Geothermometry

Fluid inclusion geothermometry, now recognized as one of the most accurate and widely applicable techniques for determining the temperatures at which a crystal formed or recrystallized, consists of determining the temperature at which a heterogeneous fluid inclusion homogenizes. In practice, a sample is heated while being viewed on a microscope stage until the liquid and a coexisting bubble that occupy the inclusion at room temperature homogenize and fill the inclusion as a single fluid. Filling is usually accomplished by disappearance of the bubble, but it may also occur by conversion of the liquid phase to vapor. The actual filling temperature is, in practice, often reproducible to ~1°C, but it represents a minimum value for the temperature of formation, because, in general, an appropriate pressure correction is necessary. In low-temperature deposits formed from dense, high-salinity fluids at shallow depths (e.g., many Pb-Zn ores in carbonate rocks), corrections are usually <25°C, but, in high-temperature ores formed from low-salinity fluids at depths >10 km, corrections may exceed 300°C. The correction procedure is illustrated in the temperature density diagram for H_2O shown in Figure 8.25. The heavy curve extending from G (gas) to L (liquid) represents the boundary of the two-phase field for pure H_2O and thus defines the filling temperatures for H_2O inclusions of various densities. Thus, an inclusion with a 70% fluid-filling (density = 0.7 if pure H_2O) would homogenize at 300°C (T_H, P_H). If, however, independent geologic information indicated that the actual pressure at the time of trapping (P_T) was 1,600 bars, then the true trapping temperature (T_T) was actually 470°C (i.e., the temperature at which the 0.7 density coordinate cuts the 1,600 isobar). If the inclusion were found to contain a 20% NaCl solution (density + 1.15 at 20°C) by a freezing-point determination, the pres-

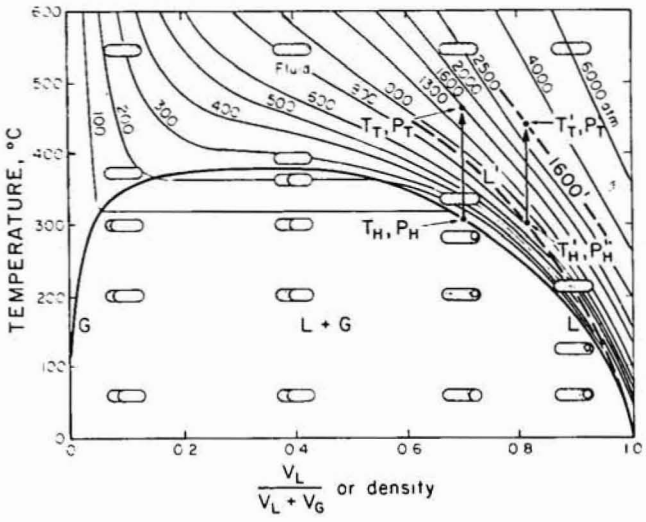

FIGURE 8.25 Temperature-density diagram for the system H_2O, illustrating the method of applying pressure corrections in fluid inclusion studies. The heavy solid line is the boundary of the two-phase field for pure H_2O and represents the homogenization temperature for inclusions filled with water. The light solid lines are isobars for pure H_2O. The heavy dashed line L illustrates the position of the two-phase field for H_2O with 20 wt % NaCl, and the dashed line labeled 1600′ represents the 1,600 atm isobar for a 20 wt % NaCl solution. The pressure correction procedure is described in the text.

sure correction would have to be made from another family of curves (examples of which are shown in the heavy dashed curves in Figure 8.25) representing the two-phase boundary and isobars for a 20% NaCl solution. The two-phase boundary for this liquid is shown by the heavy dashed curve (L′). The isobars for salt solutions are not well known, but the 1,600 isobar for a 20% NaCl solution is shown schematically as the heavy dashed 1,600′ curve. Accordingly, the corrected trapping temperature (T'_T, P'_T) of an inclusion that homogenized at 300°C (T'_H, P'_H) and that contains a 20% NaCl solution is 450°C.

The data employed in making pressure corrections were originally derived by Lemmlein and Klevstov (1961) and later summarized by Potter (1977). Since halite solubility in water is temperature dependent, determination of the temperature at which any daughter halite crystals dissolve establishes a minimum for the initial temperature of trapping.

8.5.6 Applications of Fluid Inclusion Studies

Fluid inclusion geothermometry has been extensively employed in determining the temperatures of ore mineral formation. However, Roedder (1977, 1979, 1984) has pointed out that there are several other uses for fluid inclusion studies, including mineral exploration and even the determination of geologic age relations. For additional information on the examples noted in the follow-

ing discussion, the reader is directed to Roedder's papers and the references at the end of this chapter.

The two most obvious applications of fluid inclusion studies are the determination of the temperature of ore formation or recrystallization and the determination of the salinity of the fluid entrapped. The study of fluid inclusions in epigenetic ores often has revealed that the temperatures at which the ores were emplaced were different from the temperatures recorded in fluid inclusions in the enclosing host rocks. Furthermore, temperature variations both temporal and spatial in origin have been observed within single ore deposits (e.g., Creede, Colorado; Panasqueira, Portugal; Casapalca, Peru) and even within different growth zones of single crystals. In such cases, the temperature differences observed may be employed either to locate "blind" ore bodies or to extend known ones. Variations within a mineralized zone may also serve to define directions of ore fluid movement, to aid in the interpretation of paragenesis, and as records of the changing nature of the ore fluid as a function of time. Since ore-forming brines are often more concentrated than fluids not associated with ores, trends in salinity obtained from freezing-point measurements may supplement temperature data in the exploration or extension of ore deposits.

In some districts, veins formed only during one episode, or of only one affinity, carry mineralization, whereas other veins of identical gangue mineralogy are barren. In some instances (e.g., Sadonsk, Soviet Union; Cobalt, Ontario), the fluid inclusion data are significantly different for the two types of veins and thus can be used to aid in exploration. In structurally complex areas cut by several generations of veins of similar mineralogy, fluid inclusion data may help identify segments of individual veins and may aid in clarifying the chronological relationships between veins. Similarly, the chronology of crosscutting veins of similar mineralogy may be clarified, because natural decrepitation (i.e., bursting due to heating) or halo effects may be observed in the fluid inclusions of the older vein. In structurally complex areas, detailed sampling may yield information that places constraints on the metamorphism and even the history of uplift (Hall, Bodnar, and Craig (1991).

During weathering and erosion of ore deposits, resistant gangue minerals such as quartz are preserved with fluid inclusions intact in the gossan, the residual soils, in placer gold grains, and in other stream sediments derived during erosion. The fluid inclusions in such quartz may be used as an aid in deciphering the nature of the original deposit and even its location.

Clearly, the many potential uses of fluid inclusion studies will result in their increasing application to the study of ore deposits.

REFERENCES

Barker, C. E., and Kopp, O. C., eds. (1991). Luminescence microscopy and spectroscopy: quantitative and qualitative aspects. *Soc. Econ. Paleon. and Mineral.*

Barton, P. B., Bethke, P. M., and Roedder, E. (1977). Environment of ore deposition in

the Creed mining district, San Juan Mountains, Colorado: Part III. Progress toward interpretation of the chemistry of the ore-forming fluid for the OH vein. *Econ. Geol.* **72**, 1–24.

Barton, P. B., and Skinner, B. J. (1979). Sulfide Mineral Stabilities. In H. L. Barnes (ed.), *Geochemistry of Hydrothermal Ore Deposits*, 2nd ed. Wiley-Interscience, New York.

Bodnar, R. J., and Sterner, S. M. (1987). Synthetic fluid inclusions. In G. C. Ulmer and H. L. Barnes (eds.), *Hydrothermal Experimental Techniques*. Wiley-Interscience, New York, pp. 423–457.

Brooker, D. D., Craig, J. R., and Rimstidt, J. D. (1987). Ore metamorphism and pyrite porphyroblast development at the Cherokee Mine, Ducktown, Tennessee. *Econ. Geol.* **82**, 72–86.

Brumby, G. R., and Shepherd, T. J. (1978). Improved sample preparation for fluid inclusion studies. *Mineral. Mag.* **42**, 297–298.

Craig, J. R. (1973). Pyrite-pentlandite assemblages and other low temperature relations in the Fe-Ni-S system. *Am. J. Sci.* **273A**, 496–510.

Cunningham, C. F. (1976). Fluid inclusion geothermometry. *Geol. Rundsch.* **66**, 1–9.

Ebers, M. L., and Kopp, O. C. (1979). Cathodoluminescence microstratigraphy in gangue dolomite, the Mascot-Jefferson City District, Tennessee. *Econ. Geol.* **74**, 908–918.

Francis, C. A., Fleet, M. E., Misra, K. C., and Craig, J. R. (1976). Orientation of exsolved pentlandite in natural and synthetic nickeliferous pyrrhotite. *Am. Mineral.* **61**, 913–920.

Hall, D. L., Bodnar, R. J., and Craig, J. R. (1991). Fluid inclusion constraints on the uplift history of the metamorphosed massive sulfide deposits at Ducktown, Tennessee. *J. of Metam. Geol.* **9**, 551–565.

Hall, D. L., Sterner, S. M., and Bodnar, R. J. (1988). Freezing point depression of NaCl-KCl-H_2O solutions. *Econ. Geol.* **83**, 197–202.

Hutchison, M. N., and Scott, S. D. (1979). Application of the sphalerite geobarometer to Swedish Caledonide and U.S. Appalachian metamorphosed massive sulfide ores (abs.). *Symposium Volume on Caledonian-Appalachian Stratabound Sulphides* Trondheim, Norway, pp. 14–15.

Hutchison, M. N., and Scott, S. D. (1981). Sphalerite geobarometry in the Cu-Fe-Zn-S system. *Econ. Geol.* **76**, 143–153.

Kelly, D. P., and Vaughan, D. J. (1983). Pyrrhotite-pentlandite ore textures: a mechanistic approach. *Mineral Mag.* **47**, 453–463.

Kelly, W. C., and Turneaure, F. S. (1970). Mineralogy, paragenesis, and geothermometry of the tin and tungsten deposits of the Eastern Andes, Bolivia. *Econ. Geol.* **65**, 609–680.

Kostov, I., and Mincheeva-Stefanova, J. (1981). Sulphide Minerals: Crystal Chemistry Paragenesis and Systematics. *Bulgarian Acad. Sci.*

Kretschmar, U., and Scott, S. D. (1978). Phase relations involving arsenopyrite in the system Fe-As-S and their application. *Can. Mineral.* **14**, 364–386.

Lemmlein, G. G., and Klevtsov, P. V. (1961). Relations among the principal thermodynamic parameters in a part of the system H_2O-NaCl. *Geokhimiya* 2, 133–142 (in Russian); trans. in *Geochemistry* **6**, 148–158.

Lindsley, D. H., ed. (1991). Oxide minerals: petrologic and magnetic significance. Revs. in Mineralogy **25**, *Min. Soc. America*.

Lusk, J., and Ford, C. E. (1978). Experimental extension of the sphalerite geobarometer to 10 bar. *Am. Mineral.* **63**, 516–519.

Marshall, D. J. (1988). *Cathodoluminescence of Geologic Materials.* Unwin-Hyman, Boston.

McLimans, R. K., Barnes, H. L., and Ohmoto, H. (1980). Sphalerite of the Upper Mississippi Valley zinc-lead district, Southwest Wisconsin. *Econ. Geol.* **75**, 351–361.

Meyers, W. J. (1978). Carbonate cements: their regional distribution and interpretation in Mississippian limestones of southwestern New Mexico. *Sedimentology* **25**, 371–400.

Naldrett, A. J., (1989). *Magmatic Sulfide Deposits.* Oxford Monogr. on Geology and Geophysics No. 14., Oxford Univ. Press, New York.

Naldrett, A. J., Craig, J. R., and Kullerud, G. (1967). The central portion of the Fe-Ni-S system and its bearing on pentlandite exsolution in iron-nickel sulfide ores. *Econ. Geol.* **62**, 826–847.

Nickel, E. (1978). The present status of cathode luminescence as a tool in sedimentology. *Min. Sci. Eng.* **10**, 73–100.

Potter, R. W. (1977). Pressure corrections for fluid-inclusion homogenization temperatures based on the volumetric properties of the system $NaCl\text{-}H_2O$. *Journ. Res. U.S. Geol. Surv.* **5**, 603–607.

Potter, R. W., Clynne, M. A., and Brown, D. L. (1978). Freezing point depression of aqueous sodium chloride solutions. *Econ. Geol.* **73**, 284–285.

Ribbe, P. H., ed. (1974). *Sulfide Mineralogy.* Mineral. Soc. Short Course Notes, Vol. 1, Washington, D.C.

Roedder, E. (1962). Ancient fluids in crystals. *Sci. Am.* (Oct. 1962), 38–47.

_____. (1968). The noncolloidal origin of "colloform" textures in sphalerite ores. *Econ. Geol.* **63**, 451–471.

_____. (1972). Composition of Fluid Inclusions. In M. Fleischer (ed.), *Data of Geochemistry.* 6th ed. U.S. Geological Survey Prof. Paper 440-JJ.

_____. (1976). Fluid-inclusion evidence on the genesis of ores in sedimentary and volcanic rocks. In K. H. Wolf (ed.), *Handbook of Stratabound and Stratiform Ore Deposits.* Elsevier, Amsterdam, Vol. 2, pp. 67–110.

_____. (1977). Fluid inclusions as tools in mineral exploration. *Econ. Geol.* **72**, 503–525.

_____. (1979). Fluid inclusions as samples of ore fluids. In H. L. Barnes (ed.), *Geochemistry of Hydrothermal Ore Deposits*, 2nd ed. Wiley-Interscience, New York, pp. 684–737.

_____. (1984). Fluid Inclusions. Reviews in Mineralogy No. 12 Mineralogical Society of America, Washington, D.C. 644 pp.

_____. (1990). Fluid Inclusion analysis—prologue and epilogue. *Geochimica et Cosmochimica Acta*, **54**, 495–507.

Rumble, D., ed. (1976). *Oxide Minerals.* Min. Soc. Am. Short Course Notes, Vol. 3, Washington, D.C.

Scott, S. D. (1973). Experimental calibration of the sphalerite geobarometer. *Econ. Geol.* **68**, 466–474.

Scott, S. D., and Barnes, H. L. (1971). Sphalerite geobarometry and geothermometry. *Econ. Geol.* **66**, 653–669.

Shepherd, T., Rankin, A. H., and Alderton, D. H. M. (1985). *A Practical Guide to Fluid Inclusion Studies.* Blackie, London.

Vaughan, D. J., and Craig, J. R. (1978). *Mineral Chemistry of Metal Sulfides.* Cambridge University Press, Cambridge, England.

Vaughan, D. J., and Ixer, R. A. (1980). Studies of the sulfide mineralogy of North Pennine ores and its contribution to genetic models. *Trans. Inst. Min. Metall.* **89**, B99–B109.

Yund, R. A., and Kullerud, G. (1966). Thermal stability of assemblages in the Cu-Fe-S system. *J. Petrol.* 7, 454–488.